NAVAL POSTGRADUATE SCHOOL
Monterey, California

DTIC
ELECTE
FEB 2 8 1994
S
A

THESIS

MINE AVOIDANCE AND LOCALIZATION FOR UNDERWATER VEHICLES
USING CONTINUOUS CURVATURE PATH GENERATION AND NON-LINEAR
TRACKING CONTROL

by

Dean J. Cottle

September 1993

Thesis Advisor: Anthony J. Healey

Approved for public release: Distribution unlimited.

94-06456

REPORT DOCUMENTATION PAGE

Form Approved
OMB No 0704-0188

1a REPORT SECURITY CLASSIFICATION UNCLASSIFIED	1b RESTRICTIVE MARKINGS
2a SECURITY CLASSIFICATION AUTHORITY	3 DISTRIBUTION/AVAILABILITY OF REPORT Approved for public release;
2b. DECLASSIFICATION/DOWNGRADING SCHEDULE	distribution unlimited.

4 PERFORMING ORGANIZATION REPORT NUMBER(S)	5 MONITORING ORGANIZATION REPORT NUMBER(S)

6a. NAME OF PERFORMING ORGANIZATION Naval Postgraduate School	6b OFFICE SYMBOL (If applicable) ME	7a. NAME OF MONITORING ORGANIZATION Naval Postgraduate School
6c ADDRESS (City, State, and ZIP Code) Monterey, CA 93943-5000		7b. ADDRESS (City, State, and ZIP Code) Monterey, CA 93943-5000
8a. NAME OF FUNDING/SPONSORING ORGANIZATION	8b OFFICE SYMBOL (If applicable)	9 PROCUREMENT INSTRUMENT IDENTIFICATION NUMBER
8c. ADDRESS (City, State, and ZIP Code)		10 SOURCE OF FUNDING NUMBERS

PROGRAM ELEMENT NO	PROJECT NO	TASK NO	WORK UNIT ACCESSION NO

11 TITLE (Include Security Classification)

MINE AVOIDANCE AND LOCALIZATION FOR UNDERWATER VEHICLES USING CONTINUOUS CURVATURE PATH GENERATION AND NON-LINEAR TRACKING CONTROL

12 PERSONAL AUTHOR(S)
Cottle, Dean J.

13a TYPE OF REPORT Thesis	13b TIME COVERED FROM 6/92 TO 9/93	14 DATE OF REPORT (Year,Month,Day) September 1993	15 PAGE COUNT 75

16 SUPPLEMENTARY NOTATION
The views expressed in this thesis are those of the author and do not reflect the official policy or position of the Department of Defense or the U.S. Government.

17 COSATI CODES			18 SUBJECT TERMS (Continue on reverse if necessary and identify by block number)
FIELD	GROUP	SUB-GROUP	Mine avoidance and localization; Autonomous underwater vehicles (AUV); Autopilot and guidance of AUV II; Sliding mode control

19 ABSTRACT (Continue on reverse if necessary and identify by block number)

Many underwater vehicles have been designed to follow a straight path using linear approximations about that path. Tracking a dynamic path of arbitrary but continuous curvature may often be desired. This will require a nonlinear controller with enhanced robustness properties. One point of this thesis is to show how nonlinear control using sliding modes may be applied to follow a dynamic path.

In a mine warfare setting using Autonomous Underwater Vehicles (AUVs), reflexive maneuvers will be required for mine avoidance. This thesis presents one way in which paths for mine avoidance maneuvers may be generated automatically and used as inputs to the nonlinear tracking control system of the vehicle. It has been shown through simulation that a random minefield can be traversed by an AUV while localizing and avoiding detected mines using these control concepts.

20 DISTRIBUTION/AVAILABILITY OF ABSTRACT [X] UNCLASSIFIED/UNLIMITED ☐ SAME AS RPT. ☐ DTIC USERS	21 ABSTRACT SECURITY CLASSIFICATION UNCLASSIFIED
22a NAME OF RESPONSIBLE INDIVIDUAL Anthony J. Healey.	22b TELEPHONE (Include Area Code) 408 656-2033 22c OFFICE SYMBOL ME/HY

DD Form 1473, JUN 86   Previous editions are obsolete   SECURITY CLASSIFICATION OF THIS PAGE

S/N 0102-LF-014-6603   Unclassified

MINE AVOIDANCE AND LOCALIZATION FOR UNDERWATER VEHICLES USING CONTINUOUS CURVATURE PATH GENERATION AND NON-LINEAR TRACKING CONTROL

by

Dean J. Cottle

Lieutenent Commander, United States Navy
B.S., United States Naval Academy, 1980

Submitted in partial fulfillment of the
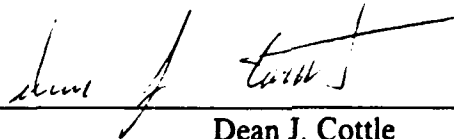requirements for the degrees of

MASTERS OF SCIENCE IN MECHANICAL ENGINEERING
and
MECHANICAL ENGINEER
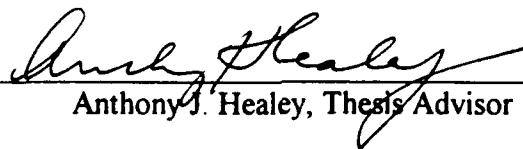
from the

NAVAL POSTGRADUATE SCHOOL

September 1993

Author: _____
Dean J. Cottle

Approved by: _____
Anthony J. Healey, Thesis Advisor

_____
Matthew D. Kelleher, Chairman,

Department of Mechanical Engineering

_____
Richard S Elster, Dean of Instruction

ABSTRACT

Many underwater vehicles have been designed to follow a straight path using linear approximations about that path. Tracking a dynamic path of arbitrary but continuous curvature may often be desired. This will require a nonlinear controller with enhanced robustness properties. One point of this thesis is to show how nonlinear control using sliding modes may be applied to follow a dynamic path.

In a mine warfare setting using Autonomous Underwater Vehicles (AUVs), reflexive maneuvers will be required for mine avoidance. This thesis presents one way in which paths for mine avoidance maneuvers may be generated automatically and used as inputs to the nonlinear tracking control system of the vehicle. It has been shown through simulation that a random minefield can be traversed by an AUV while localizing and avoiding detected mines using these control concepts.

TABLE OF CONTENTS

LIST OF FIGURES

ACKNOWLEDGMENTS

I would like to thank my thesis advisor Professor Anthony J. Healey for his expert assistance and direction during the development of this work. His ability to see through the algebra mistakes corrected many problems. I would also like to thank Professor Yotaka Kanayama for his work in path planning. It was his course in Advanced Robotics that sparked my interest in applying his work to AUV control.

I would also like to thank my best friend and wife, Jean. Without her support, patience, and love this thesis would not have been possible. I would also like to thank my children Kenneth, Brad, Justin and Tiffany. I was not able to spend much time with them lately. Their understanding made it easier on me.

I. INTRODUCTION

A. BACKGROUND AND MOTIVATION

Autonomous Underwater Vehicles (AUVs) are unmanned and independent craft with respect to power and control. Unlike Remotely Operated Vehicles (ROVs) which require tethered cables for external power and control, AUVs require no external interface. AUVs are receiving interest by both naval and civilian activities operating in the ocean environment. Their missions include area search, survey data gathering, and mobile sensor placement, as well as, remote sensor capabilities for both surface ships and submarines. Clearly, these unmanned vehicles will be used to extend man's presence in this hostile environment.

Mission planners use waypoint path planning to direct the motion of AUVs. These waypoints are selected to avoid known undersea obstacles with a minimum safety distance and are given a corridor with a distance either side of the directed path. A speed of advance (SOA) is used so that the planner knows were the vehicle is supposed to be along the path at all times. This allows flexibility in water management to allow other vehicles access as soon as the area is clear. But, if an unknown obstacle is present while following the planned path these AUVs must maneuver around the obstacle while keeping the vehicle as close to the directed path as possible.

Autonomous vehicle studies, up till now, have focused on following a path defined by straight lines. Linear controls have been used extensively in these situations assuming small motions about a nominal straight path. The simplest guidance scheme used waypoint aiming, sometimes referred to as line of sight steering, (as in "proportional navigation") with a separate constant speed controller. A new heading was calculated to the waypoint

based on current position estimates. This design allowed the vehicle to wander off the proposed track and could produce a significant heading difference from the desired when approaching the waypoint [Ref. 1]. Due to the added distance required to travel in these cases synchronous time of arrival is difficult. This design is improved by adding a speed controller to change speed as necessary to reach the waypoint on time.

At the next level of complexity, cross track error can be used to control heading to regain track with a separate speed controller. But again, these systems inherently maintain a straight track which may be sufficient in open ocean, but could cause problems in the performance of obstacle avoidance maneuvers in confined waters. There may be certain times when a vehicle needs the ability to follow a nonlinear path, as when required to reflexively avoid obstacles. None of the present control schemes proposed have that ability.

When tracking a straight line the path velocity is constant thus the state variables' rate and acceleration don't change. To follow a nonlinear path requires a nonlinear control design and a more robust control system capable of handling the additional dynamics involved. Nonlinear control theory has only recently been developed and is not yet well established for a Multiple Input-Multiple Output (MIMO) control system. [Ref. 2]

The purpose of this thesis is therefore two fold: firstly, to raise the precision in vehicle motion control capability and explore the use of nonlinear tracking control theory for submarine path tracking; and secondly, to generate continuous curvature paths as desired paths that would balance the tracking of the nominal path while avoiding detected obstacles.

B. OVERVIEW OF NAVAL POSTGRADUATE SCHOOL AUV PROGRAM

The AUV program at the Naval Postgraduate School (NPS) began in 1987 with the sponsorship of the Naval Surface Warfare Center. The project involves joint effort from the Mechanical Engineering, Computer Science, and Electrical and Computer Engineering Departments and is focused on the control, at both the Mission and Execution levels of an experimental vehicle - the NPS AUV II.

The NPS AUV II is a seven foot autonomous vehicle. It was designed using the Total Ships System Engineering approach. This integrated approach involved an iterative design spiral weighing tradeoffs in the following systems: Hull, Energy Storage and Power Plant, Vehicle Motion Control, Sensor Suite, Navigation and Guidance, and Machinery Monitoring, [Ref. 3]. Figure I-1 shows the configuration of the AUV II and its internal equipment arrangement. The AUV II contains its own internal power supply using rechargeable batteries and its own guidance, control and navigation computers for autonomous operation. It has a sonar suite that consists of a 200 KHz fathometer, a 750 KHz high resolution sector scanning sonar and a 1 MHz pencil beam profiling sonar. No external tether is required.

The AUV II guidance system consists of an autopilot and associated guidance laws. The autopilot is responsible for stable control of the vehicle in achieving desired course, speed and depth. The guidance law converts the vehicle position and orientation into a global reference, combines this with the desired position and orientation thus generating a global error signal for the autopilot. Vehicle orientation control is accomplished with the use of bow and stern rudders and planes as well as four cross body thrusters. Longitudinal velocity is controlled through shaft RPM, and depth control through bow and stern planes.
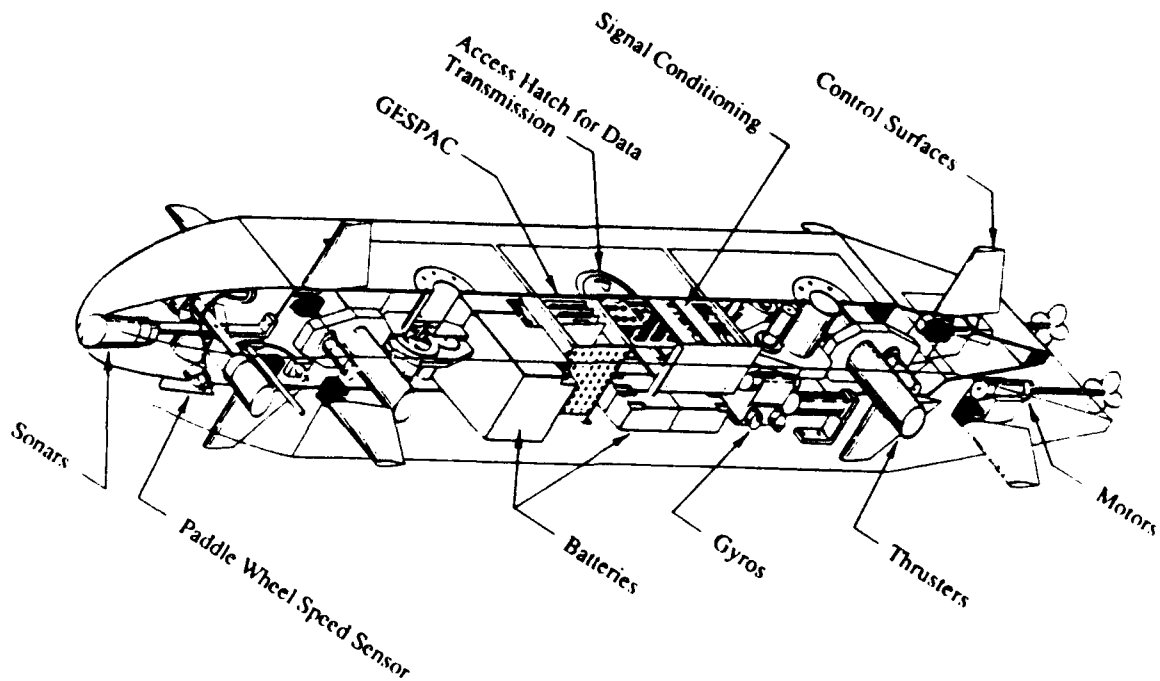
3

Figure I-1.   AUV II, Internal Equipment Arrangement

C. SCOPE OF THIS THESIS

This thesis addresses only a small area of the autonomous control problem for the NPS AUV II dealing with horizontal plane nonlinear control using Multiple Input-Multiple Output (MIMO) Sliding Mode Control to follow continuously changing curved tracks. First we develop the nonlinear controller for the AUV and demonstrate its effectiveness at following nonlinear paths. We then develop a path generation routine which changes curvature of the path based on sensor measurements and orientation parameters. This is then applied, in simulation, to reflexive obstacle avoidance in a mine search and localization mission. From this routine the vehicle's controller is provided a path for input.

This path planning scheme is not based on an optimization which would require extensive computational time. This scheme will react to its environment. An algorithm that

4

is totally reflexive based on current information would provide a control signal within the step time of the execution level controller (0.1 sec), [Ref. 4]. In practice, this system will employ sonar detection of obstacles within its field of view and use range and bearing to calculate the avoidance command. This will be added to the steering order to regain the nominal path and generate a steering function to create the avoidance path for the AUV to follow.

D. THESIS OUTLINE

Chapter II will discuss the theoretical background of sliding mode control. It will include the conditions of existence and stability of the sliding surface, sliding surface design, and sliding mode control.

Chapter III will present the AUV equations of motion and develop the control law for the nonlinear model. Sliding mode parameter selection is critical to the operation of the sliding surface. Parameter selection will be discussed and several simulation runs following curved paths will be demonstrated.

Chapter IV will present the theoretical background for continuous curvature track generation. This will include kinematics, path keeping, and obstacle avoidance algorithm generation.

Chapter V demonstrates the effectiveness of the AUV to follow a track generated from the obstacle avoidance routine using the control system designed. Discussions of its limitations will be included.

Chapter VI presents the conclusions of this research and provides recommendations for future work.

II.   THEORETICAL BACKGROUND OF SLIDING MODE CONTROL

A.   GENERAL

In a system, modeling imprecision comes from uncertainty about the system and the simplified representation of the dynamics involved. Modeling inaccuracies can have strong adverse effects on the performance of control systems. There are two approaches to deal with this problem: use adaptive control, which modifies or updates the parameters within the controller, or use a robust control that is relatively unaffected by system parameter inaccuracies.

One approach to robust control is through the use of a sliding mode methodology. The premise behind this method is that it is easier to control a 1st order nonlinear or uncertain system than it is to control a general system described by an nth order differential equations. In effect we replace an nth order system with an equivalent 1st order problem. It is then possible to show that "perfect" performance is attainable in the equivalent system even in the presence of arbitrary parameter inaccuracies. But, there is a price. Extremely high control activity is required which also can add to the modeling uncertainty. Thus a tradeoff can and should be evaluated balancing reduced control activity at the cost of acceptable tracking performance for given parameter uncertainty. In this chapter, an outline of the design methodology for control of a general nonlinear plant is given as an introduction to Sliding Mode Control.

B.   SLIDING SURFACE DESIGN

The objective is to find a sliding mode control law for an nth order system of the form

$$x^{(n)} = f(\mathbf{x}) + b(\mathbf{x}) \cdot u \tag{II-1}$$

where the scalar x is the output of interest ,the scalar u is the control input, and

$$\mathbf{x} = [x \quad \dot{x} \quad . \quad . \quad x^{(n-1)}] \tag{II-2}$$

is the state vector. The functions $f(\mathbf{x})$ and $b(\mathbf{x})$ are not exactly known, but the inaccuracies are bounded. The problem then is to get the output $\mathbf{x}$ to track a specific time varying command, $\mathbf{x}_d$, in the presence of model uncertainty. We assume that the system is initially in equilibrium where

$$\mathbf{x}(0) = \mathbf{x}_d(0). \tag{II-3}$$

Let $\tilde{x} = x - x_d$ be the tracking error of the single variable x. If we define a sliding surface by

$$\sigma(x,t) = \left(\lambda \tfrac{d}{dt} + 1\right)^{n-1} \tilde{x} = 0 \tag{II-4}$$

and λ is defined as a positive constant, then if n=2 the sliding surface becomes

$$\sigma = \lambda \dot{\tilde{x}} + \tilde{x}. \tag{II-5}$$

σ is then the weighted sum of the position and velocity errors. Now the problem of tracking $x=x_d$ is equivalent to remaining on the surface (σ=0) for t>0 given the initial conditions. Therefore σ=0 represents a linear differential equation with a unique solution $\tilde{x} = 0$ and an eigenvalue $1/\lambda$. The scalar σ can be kept at zero using the control u such that when $\sigma \neq 0$,

$$\frac{1}{2}\frac{d}{dt}\sigma^2 \leq -\eta|\sigma| \tag{II-6}$$

where η is a positive constant. This states that the rate of change of the squared "distance" to the surface decreases along all paths. This constrains the trajectory to point to the surface and once on the surface to remain on the surface. Thus even with disturbances and parameter inaccuracies the system maintains σ on the surface and tracking errors tend exponentially to zero with a time constant of (n-1)λ.[Ref. 5]

7

In summary, the idea behind Equations (II-4) and (II-6) is to follow a well behaved function of the tracking error and select the feedback control law u in Equation (II-1) such that σ^2 remains a Lyapunov-like function of the closed loop system despite disturbances and model imprecisions.

C. SLIDING MODE CONTROL

To illustrate this process consider the example of a scalar system of single control input u

$$\ddot{x} = f(x) + u \tag{II-7}$$

where x is the scalar output, and f is the nonlinear time varying system dynamics which are not exactly known but are estimated as $\hat{f}$. The estimation error in f is assumed to be bounded by a function F where

$$F = f - \hat{f}. \tag{II-8}$$

For the system to track $x(t) = x_d(t)$, we use Equation (II-4) to define the sliding surface.

$$\sigma = \lambda \dot{x} + x. \tag{II-9}$$

We then have:

$$\sigma = \lambda \dot{\tilde{x}} + \tilde{x} \tag{II-10}$$

and differentiating with respect to time,

$$\dot{\sigma} = \lambda \ddot{x} - \lambda \ddot{x}_d + \dot{\tilde{x}} = \lambda(f + u - \ddot{x}_d) + \dot{\tilde{x}}. \tag{II-11}$$

As $\dot{\sigma}$ approaches zero the estimate of the control law then becomes:

$$\hat{u} = (-\hat{f} + \ddot{x}_d) - \lambda^{-1}\dot{\tilde{x}}. \tag{II-12}$$

In order to satisfy the sliding condition of Equation (II-6) in the presence of the uncertainty in f, a discontinuous term must be added to $\hat{u}$ to drive it back to the surface.

The hyperbolic tangent function will be used as the switching term.

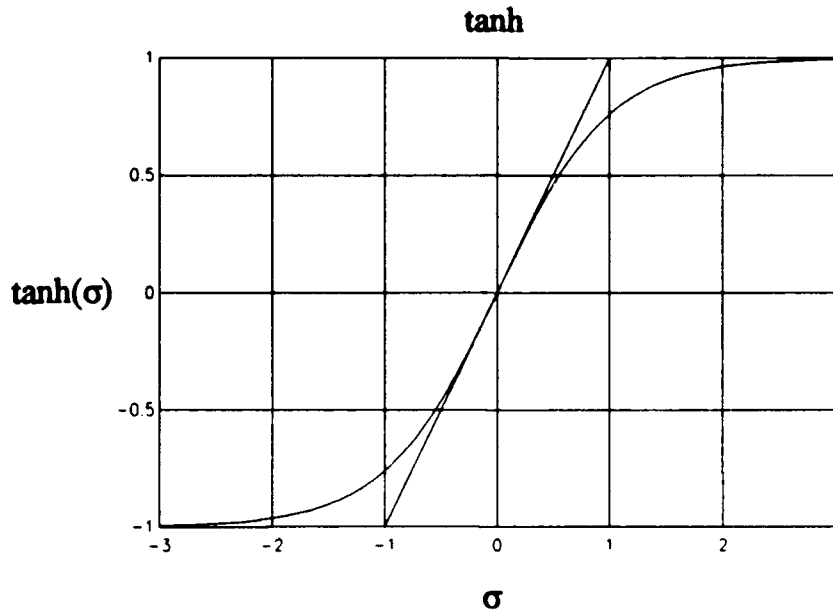$$u = \hat{u} - k\tanh(\sigma) \qquad\qquad\qquad\text{(II-13)}$$

Figure II-1.   Hyperbolic tangent function characteristics.

It can be seen that this function provides a smooth transition between states and that as the magnitude of σ gets larger the contribution to u increases. In the case where σ is not zero, $\tanh(\sigma)$ switches smoothly to ± 1 resulting in

$$\frac{1}{2}\frac{d}{dt}\left(\sigma^2\right) = \sigma\cdot\dot{\sigma} = \lambda[(f - \hat{f}) - k\cdot\tanh(\sigma)]\cdot\sigma \qquad\text{(II-14)}$$

when $k \geq \dfrac{(|F| + \eta)}{\tanh(\sigma_o)}$ is selected.

$$\frac{1}{2}\frac{d}{dt}\left(\sigma^2\right) = \lambda[F - k\tanh(\sigma)]\cdot\sigma \leq -\eta\cdot|\sigma| \qquad\text{(II-15)}$$

This expression is always decreasing provided $|\sigma| > \sigma_o$. and given that $|F|$ is the upper bound on F. Choosing k to be large enough, ensures robust bounded stability of the system. Here we see the main advantage in transforming the original tracking problem into

9

a simple first order system. The simple control strategy of pushing hard enough in the opposite direction of the error works for a first order system but, does not necessarily work in higher order systems.

In order to design the control law for a single input-single output system the measurable variable y must be identified and related to the state variables through a constant parameter H.

$$y = Hx \tag{II-16}$$

The error function, σ, is expressed as a function of the measurable and desired parameters,

$$\sigma = y - y_d = Hx - y_d = H\tilde{x}, \tag{II-17}$$

with the system dynamics of the form

$$\dot{x} = f(x) + bu, \tag{II-18}$$

where b is a constant scalar. H may appear to be a nuisance in this simple problem but is necessary when dealing with MIMO systems working in real space. Taking the derivative of the error function and setting it equal to the sliding surface control function the following form is achieved

$$\dot{\sigma} = H(f + bu) - \dot{y}_d = -\eta \tanh(\sigma) \tag{II-19}$$

resulting in the control input

$$u = (Hb)^{-1}[(\dot{y}_d - Hf) - \eta \tanh(\sigma)]. \tag{II-20}$$

Here we see that the control input is a function of the difference between the desired velocity and the product Hf, as well as the proximity to the sliding surface.

In more complex multivariable systems it may not be this easy to isolate the control input. The ability to solve for u may require a higher order σ to be used until the control input can be identified.

$$\sigma = \tilde{x} + \lambda_1 \dot{\tilde{x}} + \lambda_2 \ddot{\tilde{x}} + \dots \tag{II-21}$$

10

The use of Equation (II-20) with the system in Equation (II-18) then leads to the dynamic response of σ given by Equation (II-19) but driven by uncertainties in f, and leads to both $\sigma(t)$ and therefore $\tilde{x}$ tending to a bounded constant as $t \rightarrow \infty$.

III. SLIDING MODE CONTROL FOR AUVS IN THE HORIZONTAL PLANE

A. EQUATIONS OF MOTION

The design of the NPS AUV II tracking control system begins with identifying the equations of motion of a physics based model. The six generalized equations of motion for a submerged vehicle are found in *Principles of Naval Architecture* [Ref. 6]. In developing the model for the AUV II several assumptions were made to simplify and limit ourselves to the horizontal plane. The assumptions are summarized below:

1. The AUV II is neutrally buoyant: $W=B$.

2. The AUV II is symmetrically loaded in the transverse direction ($y_G=0$ and $y_B=0$), and the vertical center of buoyancy is midway between the top and bottom of the AUV II ($z_B=0$).

3. The counter-rotating propellers produce no yaw moment (Nprop=0).

4. The products of inertia about the body system are zero because the AUV II possesses two axes of symmetry.

5. The AUV II acceleration rates are small enough that propeller slip can be neglected.

6. The effect of cross-coupled hydrodynamic added mass coefficients can be neglected in most cases, again because of the AUV II geometric symmetry.

The resulting generalized equations of motion for horizontal plane motion including surge, sway, and yaw are presented below, where n and DR are generalized controls.

12

$$(m - X_{\dot{U}})\dot{U} = (mVR - X_{UU}U|U| + X_{PROP}n^2)$$
$$(m - Y_{\dot{V}})\dot{V} = (-mRU + Y_V VU + Y_R RU + (Y_{DRb} + Y_{DR_s})U^2 DR) \qquad \text{(III-1)}$$
$$(I_{zz} - N_{\dot{R}})\dot{R} = (N_V VU + N_R RU + (N_{DRb} + N_{DR_s})U^2 DR)$$

TABLE III-1 AUV II HYDRODYNAMIC COEFFICIENTS

Coefficient	Value	Coefficient	Value
L(ft)	7.3	$\rho(\text{lbm/ft}^3)$	1.94
m(lbm)	435(lbf)/g	X_{uu}	$0.015 \cdot \tfrac{1}{2}\rho L^2$
g	32.2	X_{prop}	$X_{uu}(2.3/500)^2$
$I_{zz}(\text{ft}^4)$	45	$X_{\dot{U}}$	$-0.00282 \cdot \tfrac{1}{2}\rho L^3$
Y_v	$-0.03896 \cdot \tfrac{1}{2}\rho L^2$	N_v	$-0.00769 \cdot \tfrac{1}{2}\rho L^3$
$Y_{\dot{v}}$	$-0.03430 \cdot \tfrac{1}{2}\rho L^3$	$N_{\dot{v}}$	$-0.00178 \cdot \tfrac{1}{2}\rho L^4$
Y_R	$0.01187 \cdot \tfrac{1}{2}\rho L^3$	N_R	$-0.01022 \cdot \tfrac{1}{2}\rho L^4$
$Y_{\dot{R}}$	$-0.00178 \cdot \tfrac{1}{2}\rho L^4$	$N_{\dot{R}}$	$-0.00047 \cdot \tfrac{1}{2}\rho L^5$
Y_{DRb}	$0.02345 \cdot \tfrac{1}{2}\rho L^2$	N_{DR_s}	$-0.377 \cdot L \cdot Y_{DR_s}$
Y_{DR_s}	$0.02345 \cdot \tfrac{1}{2}\rho L^2$	N_{DRb}	$0.283 \cdot L \cdot Y_{DRb}$

The X, Y, and N terms are the hydrodynamic influence coefficients as presented by Warner [Ref. 7]. They relate the force or moment on the vehicle for a given change in the vehicle motion of interest and are often converted from nondimensional quantities involving vehicle length and forward speed. For example, the change in force in the Y direction for a given change in sway velocity or a given stern rudder angle is annotated by,

$$Y_v = \frac{1}{U}\frac{\partial Y}{\partial v} \quad \text{and} \quad Y_{DR_s} = \frac{1}{U^2}\frac{\partial Y}{\partial DRs}.$$

To relate vehicle motion to a global coordinate system a transformation is required that relates vehicle surge and sway velocities to the global velocities and yaw rate to the global Euler angle rate.

$$\dot{\Psi} = R$$

$$\dot{x} = U\cos(\Psi) - V\sin(\Psi) \tag{III-2}$$

$$\dot{y} = U\sin(\Psi) + V\cos(\Psi)$$

Most control systems deal with Equations (III.1) and (III.2) as separate guidance and autopilot systems. Though auotpilots in the past have incrementally segmented the path to effectively form a curved path, they lack of rate and acceleration terms, for feed forward, which more accurately define the curved path. But, when trying to follow a global track with sliding modes these equations are integral to each other. By coupling them together into a single function the total effect of their relationships form a single control system. This provides us with

$$
\begin{bmatrix}
(m - X_{\dot{U}}) & 0 & 0 & 0 & 0 & 0 \\
0 & (m - Y_{\dot{V}}) & 0 & 0 & 0 & 0 \\
0 & 0 & (I_{zz} - N_{\dot{R}}) & 0 & 0 & 0 \\
0 & 0 & 0 & 1 & 0 & 0 \\
0 & 0 & 0 & 0 & 1 & 0 \\
0 & 0 & 0 & 0 & 0 & 1
\end{bmatrix}
\begin{bmatrix}
\dot{U} \\ \dot{V} \\ \dot{R} \\ \dot{\Psi} \\ \dot{x} \\ \dot{y}
\end{bmatrix}
=
$$

$$
\begin{bmatrix}
mVR - X_{UU}U|U| \\
-mRU + Y_{V}VU + Y_{R}RU \\
N_{V}VU + N_{R}RU \\
R \\
U\cos(\Psi) - V\sin(\Psi) \\
U\sin(\Psi) + V\cos(\Psi)
\end{bmatrix}
+
\begin{bmatrix}
X_{PROP} & 0 \\
0 & (Y_{DRb} + Y_{DRs})U^2 \\
0 & (N_{DRb} + N_{DRs})U^2 \\
0 & 0 \\
0 & 0 \\
0 & 0
\end{bmatrix}
\begin{bmatrix}
n^2 \\ DR
\end{bmatrix}
\tag{III-3}
$$

To reduce the complexity of this equation for subsequent calculations M, $F(X)$, G and δ will replace their respective matrices to form the following equation

$$M\dot{X} = F(X) + G\delta \tag{III-4}$$

$$\dot{X} = M^{-1}\{F(X) + G\delta\} = M^{-1}F(X) + M^{-1}G\delta. \tag{III-5}$$

14

B. CONTROL INPUT DEVELOPMENT

To develop a control system to follow a path defined by global x and y coordinates there must be at least two control inputs. These two inputs will be RPM squared (n^2) for longitudinal speed control and rudder order (DR) with both bow and stern rudders operating together but in opposite directions. If Y_d is defined as the desired positions in the global system then:

$$Y_d = \begin{bmatrix} x_d \\ y_d \end{bmatrix} .$$
(III-6)

If Y is defined as the current position then the system states (X) can be related to Y by H:

$$Y = \begin{bmatrix} x \\ y \end{bmatrix} = \begin{bmatrix} 0 & 0 & 0 & 0 & 1 & 0 \\ 0 & 0 & 0 & 0 & 0 & 1 \end{bmatrix} X = HX .$$
(III-7)

To control Y to Y_d an error function is required. $\tilde{Y}$ defines the error in terms of global position.

$$\tilde{Y} = Y - Y_d = HX - Y_d$$
(III-8)

In designing the sliding surface for this system, σ will be initially set equal to the error function where it will be shown to be insufficiently rich in dynamics as required to extract the solution for δ

$$\sigma = \tilde{Y} = HX - Y_d .$$
(III-9)

Taking the derivative of σ and setting it equal to the normalized sliding surface control function the following equations are obtained.

$$\dot{\sigma} = \dot{\tilde{Y}} = H\dot{X} - \dot{Y}_d = -\eta \tanh\left(\frac{\sigma}{\varphi}\right)$$
(III-10)

$$\dot{\sigma} = HM^{-1}F(X) + HM^{-1}G\delta - \dot{Y}_d = -\eta \tanh\left(\frac{HX - Y_d}{\varphi}\right).$$
(III-11)

15

Here we see that with two states being tracked $\sigma \in \Re^{2x1}$, $\eta = \begin{bmatrix} \eta_1 & 0 \\ 0 & \eta_2 \end{bmatrix}$ and

$$\tanh\left(\frac{HX - Y_d}{\varphi}\right) = \begin{bmatrix} \dfrac{\tanh(x - x_d)}{\varphi_1} \\ \dfrac{\tanh(y - y_d)}{\varphi_2} \end{bmatrix}. \text{ Solving for } \delta$$

$$\delta = \left(HM^{-1}G\right)^{-1}\left(\dot{Y}_d - HM^{-1}F(X) - \eta\tanh\left(\frac{HX - Y_d}{\varphi}\right)\right). \tag{III-12}$$

δ is shown to be a function of the difference between the path and vehicle velocities and sliding surface control function. But

$$\left(HM^{-1}G\right) = \begin{bmatrix} 0 & 0 \\ 0 & 0 \end{bmatrix} \tag{III-13}$$

and singularly not invertable thus a control can not be found and the degree of σ must be increased.

Because no solution exists in this case, a higher order sliding surface must be used and we redefine σ as a function of position and velocity errors

$$\sigma = \tilde{Y} + \lambda\dot{\tilde{Y}} = \left(HX - Y_d\right) + \lambda\left(H\dot{X} - \dot{Y}_d\right) \tag{III-14}$$

where $\lambda = \begin{bmatrix} \lambda_1 & 0 \\ 0 & \lambda_2 \end{bmatrix}$ and are time constants associated with a desired rate of decay of positional error. Taking the derivative of σ and setting it equal to the sliding surface control function we obtain

$$\begin{aligned}
\dot{\sigma} &= \dot{\tilde{Y}} + \lambda\ddot{\tilde{Y}} = \left(H\dot{X} - \dot{Y}_d\right) + \lambda\left(H\ddot{X} - \ddot{Y}_d\right) \\
&= \left(H\left(M^{-1}F(X) + M^{-1}G\delta\right) - \dot{Y}_d\right) + \lambda\left(H\left(M^{-1}\dot{F}(X) + M^{-1}G\dot{\delta}\right) - \ddot{Y}_d\right) \\
&= -\eta\tanh\left(\frac{\sigma}{\varphi}\right)
\end{aligned} \tag{III-15}$$

The $\dot{F}(X)$ term is the derivation of $F(X)$ with respect to time. Within the matrix format this must be done using

$$\dot{F}(X) = \frac{\partial F}{\partial t} = \frac{\partial F}{\partial X}\frac{\partial X}{\partial t} = F_X\dot{X} \quad ; \quad F_X \in \Re^{6x6}, \quad \dot{X} \in \Re^{6x1} \tag{III-16}$$

16

where

$$
F_X = \begin{bmatrix}
-2X_{UU}|U| & mR & mV & 0 & 0 & 0 \\
-mR + Y_V V + Y_R R & Y_V U & (Y_R - m)U & 0 & 0 & 0 \\
N_V V + N_R R & N_V U & N_R U & 0 & 0 & 0 \\
0 & 0 & 1 & 0 & 0 & 0 \\
\cos(\Psi) & -\sin(\Psi) & 0 & -U\sin(\Psi) - V\cos(\Psi) & 0 & 0 \\
\sin(\Psi) & \cos(\Psi) & 0 & U\cos(\Psi) - V\sin(\Psi) & 0 & 0
\end{bmatrix}.
$$

(III.17)

The derivative of σ equation then becomes:

$$
\left(H\left(M^{-1}F(X) + M^{-1}G\delta\right) - \dot{Y}_d \right) + \lambda\left(H\left(M^{-1}F_X \dot{X} + M^{-1}G\dot{\delta}\right) - \ddot{Y}_d \right)
$$
$$
= -\eta\tanh\left(\frac{\sigma}{\varphi}\right)
$$

(III-18)

Inserting the equation for $\dot{X}$, realizing that $\left(HM^{-1}G\right) = \begin{bmatrix} 0 & 0 \\ 0 & 0 \end{bmatrix}$ and solving for δ we

obtain

$$
\delta = \left(\lambda HM^{-1}F_X M^{-1}G\right)^{-1} \cdot
$$

$$
\left(\left(\dot{Y}_d - HM^{-1}F(X)\right) + \lambda\left(\ddot{Y}_d - HM^{-1}F_X M^{-1}F(X)\right) - \eta\tanh\left(\frac{\sigma}{\varphi}\right) \right)
$$

(III-19)

The control variable is now a function of the differences in the path and vehicle's acceleration and velocity terms. The transformational matrix term for δ becomes

$$
HM^{-1}F_X M^{-1}G = \begin{bmatrix}
\dfrac{X_{PROP}}{m - Y_{\dot{U}}}\cos(\Psi) & -U^2\left(\dfrac{Y_{DRs} + Y_{DRb}}{m - Y_{\dot{V}}}\right)\sin(\Psi) \\
\dfrac{X_{PROP}}{m - Y_{\dot{U}}}\sin(\Psi) & U^2\left(\dfrac{Y_{DRs} + Y_{DRb}}{m - Y_{\dot{V}}}\right)\cos(\Psi)
\end{bmatrix}.
$$

(III-20)

This matrix is square and therefore invertable as long as the determinant is not zero. While Equation III-20 would normally produce the required control law, one particular condition still persists where the control is not recoverable, i.e. $Y_{DRs} = -Y_{DRb}$.

17

Physically this means that under this condition, vehicle sway motions would not be directly influenced through the rudder command and it follows that path tracking to position commands is not possible this way. To resolve this dilemma another independent control variable is introduced. The AUV II has the capability to order its rudders independently but has not incorporated this in the past. To do this, the bow and stern rudders will be decoupled and controlled independently. There must be at least as many independent control variables as there are outputs to control, otherwise the transformation matrix will not have sufficient rank and δ could not be found directly. Heading will correspondingly be added to the output variables to retain squareness in the system input-output behavior. The output vector, Y, must be redefined as

$$Y = \begin{bmatrix} \Psi \\ x \\ y \end{bmatrix} = \begin{bmatrix} 0 & 0 & 0 & 1 & 0 & 0 \\ 0 & 0 & 0 & 0 & 1 & 0 \\ 0 & 0 & 0 & 0 & 0 & 1 \end{bmatrix} X \tag{III-21}$$

and the desired path coordinates must be redefined as

$$Y_d = \begin{bmatrix} \Psi_d \\ x_d \\ y_d \end{bmatrix} . \tag{III-22}$$

The control function G and control variable δ must be redefined.

$$G\delta = \begin{bmatrix} X_{PROP} & 0 & 0 \\ 0 & U^2 Y_{DRb} & U^2 Y_{DRs} \\ 0 & U^2 N_{DRb} & U^2 N_{DRs} \\ 0 & 0 & 0 \\ 0 & 0 & 0 \\ 0 & 0 & 0 \end{bmatrix} \begin{bmatrix} n^2 \\ DRb \\ DRs \end{bmatrix} \tag{III-23}$$

Following the same procedure as previously and solving for the control input

18

$$\delta = \left(\lambda H M^{-1} F_X M^{-1} G\right)^{-1} \times$$

$$\left(\left(\dot{Y}_d - H M^{-1} F(X)\right) + \lambda\left(\ddot{Y}_d - H M^{-1} F_X M^{-1} F(X)\right) - \eta \tanh\left(\frac{\sigma}{\varphi}\right)\right) \quad \text{(III-24)}$$

Simplifying the equation,

$$\delta = \left(\lambda H M^{-1} F_X M^{-1} G\right)^{-1}\left(\dot{f} + \lambda\ddot{f} - \eta \tanh\left(\frac{\sigma}{\varphi}\right)\right), \quad \text{(III-25)}$$

where $\dot{f}$ and $\ddot{f}$ are the feed forward terms from rate and acceleration errors. The transformation matrix becomes

$$\lambda H M^{-1} F_X M^{-1} G = \begin{bmatrix} 0 & \dfrac{\lambda_1 U^2 N_{DRb}}{I_{zz} - N_{\dot{R}}} & \dfrac{\lambda_1 U^2 N_{DRs}}{I_{zz} - N_{\dot{R}}} \\[3mm] \dfrac{\lambda_2 \cos(\Psi) X_{PROP}}{m - Y_{\dot{U}}} & \dfrac{-\lambda_2 U^2 \sin(\Psi) Y_{DRb}}{m - Y_{\dot{V}}} & \dfrac{-\lambda_2 U^2 \sin(\Psi) Y_{DRs}}{m - Y_{\dot{V}}} \\[3mm] \dfrac{\lambda_3 \sin(\Psi) X_{PROP}}{m - Y_{\dot{U}}} & \dfrac{\lambda_3 U^2 \cos(\Psi) Y_{DRb}}{m - Y_{\dot{V}}} & \dfrac{\lambda_3 U^2 \cos(\Psi) Y_{DRs}}{m - Y_{\dot{V}}} \end{bmatrix}$$

$$\text{(III-26)}$$

This matrix is invertable with the following analytical solution.

$$\begin{bmatrix} 0 & \dfrac{\cos(\Psi)(m - X_{\dot{U}})}{\lambda_2 X_{PROP}} & \dfrac{\sin(\Psi)(m - X_{\dot{U}})}{\lambda_3 X_{PROP}} \\[3mm] \dfrac{-Y_{DRs}(I_{zz} - N_{\dot{R}})}{\lambda_1 U^2 (N_{DRs} Y_{DRb} - N_{DRb} Y_{DRs})} & \dfrac{-\sin(\Psi) N_{DRs}(m - Y_{\dot{V}})}{\lambda_2 U^2 (N_{DRs} Y_{DRb} - N_{DRb} Y_{DRs})} & \dfrac{\cos(\Psi) N_{DRs}(m - Y_{\dot{V}})}{\lambda_3 U^2 (N_{DRs} Y_{DRb} - N_{DRb} Y_{DRs})} \\[3mm] \dfrac{Y_{DRb}(I_{zz} - N_{\dot{R}})}{\lambda_1 U^2 (N_{DRs} Y_{DRb} - N_{DRb} Y_{DRs})} & \dfrac{\sin(\Psi) N_{DRb}(m - Y_{\dot{V}})}{\lambda_2 U^2 (N_{DRs} Y_{DRb} - N_{DRb} Y_{DRs})} & \dfrac{-\cos(\Psi) N_{DRb}(m - Y_{\dot{V}})}{\lambda_3 U^2 (N_{DRs} Y_{DRb} - N_{DRb} Y_{DRs})} \end{bmatrix}$$

$$\text{(III-27)}$$

To simplify for future calculations, the constants are combined and reduced to:

$$\begin{bmatrix} 0 & \dfrac{\cos(\Psi)M}{\lambda_2} & \dfrac{\sin(\Psi)M}{\lambda_3} \\[2mm] \dfrac{-Y_s}{\lambda_1 U^2} & \dfrac{-\sin(\Psi)N_s}{\lambda_2 U^2} & \dfrac{\cos(\Psi)N_s}{\lambda_3 U^2} \\[2mm] \dfrac{Y_b}{\lambda_1 U^2} & \dfrac{\sin(\Psi)N_b}{\lambda_2 U^2} & \dfrac{-\cos(\Psi)N_b}{\lambda_3 U^2} \end{bmatrix} \qquad \text{(III-28)}$$

This matrix is clearly singular at $U=0$ when the vehicle would be uncontrollable. This work will not address this condition. The transition to hover mode will require extensive additional research. We will operate well above this region.

Solving for each individual control input

$$\delta_1 = M\left[\frac{\cos(\Psi)}{\lambda_2}\left(\dot{f}_2 + \lambda_2 \ddot{f}_2 - \eta_2 \tanh\left(\frac{\sigma_2}{\varphi_2}\right)\right) + \frac{\sin(\Psi)}{\lambda_3}\left(\dot{f}_3 + \lambda_3 \ddot{f}_3 - \eta_3 \tanh\left(\frac{\sigma_3}{\varphi_3}\right)\right)\right]$$

$$\delta_2 = \frac{-Ys}{\lambda_1 U^2}\left(\dot{f}_1 + \lambda_1 \ddot{f}_1 - \eta_1 \tanh\left(\frac{\sigma_1}{\varphi_1}\right)\right) - \frac{\sin(\Psi)Ns}{\lambda_2 U^2}\left(\dot{f}_2 + \lambda_2 \ddot{f}_2 - \eta_2 \tanh\left(\frac{\sigma_2}{\varphi_2}\right)\right) + \frac{\cos(\Psi)Ns}{\lambda_3 U^2}\left(\dot{f}_3 + \lambda_3 \ddot{f}_3 - \eta_3 \tanh\left(\frac{\sigma_3}{\varphi_3}\right)\right)$$

$$\delta_3 = \frac{Yb}{\lambda_1 U^2}\left(\dot{f}_1 + \lambda_1 \ddot{f}_1 - \eta_1 \tanh\left(\frac{\sigma_1}{\varphi_1}\right)\right) + \frac{\sin(\Psi)Nb}{\lambda_2 U^2}\left(\dot{f}_2 + \lambda_2 \ddot{f}_2 - \eta_2 \tanh\left(\frac{\sigma_2}{\varphi_2}\right)\right) - \frac{\cos(\Psi)Nb}{\lambda_3 U^2}\left(\dot{f}_3 + \lambda_3 \ddot{f}_3 - \eta_3 \tanh\left(\frac{\sigma_3}{\varphi_3}\right)\right)$$

$$\text{(III-29)}$$

Notice that each control is dependent on the choice of sliding surface coefficients. It follows that control design parameters must be carefully selected and scaled as appropriate so that the multivariable controller becomes balanced without excessive saturation on any channel.

C. PARAMETER SELECTION PROCEDURES

The parameters λ, η, and φ are selected by the control designer based on operational characteristics of the vehicle and track. The parameter λ is a term relating the ratio of errors in the output variables' displacement and rate. This determines if the displacement or rate terms dominate on the sliding surface. If $\lambda=1$, then displacement and rate terms are equally weighted. This parameter is related to the response time constant for the particular output variable. The parameter φ controls the sensitivity to saturation of each individual

sliding surface function. Too small a value will saturate the sliding surface at small error levels and will give rise to high levels of control activity. To temper the selection of φ, we must recognize that as φ grows so do the tracking errors. Thus the control designer must select a prudent value. The parameter η is for scaling the control input. If η is not large enough, the system can become unstable when parameter uncertainty exists. Too large a value will cause chatter and too small will allow errors to propagate. The best value would be just at the point of chatter but the operator must use trial and error to find this value and in practice, sensor noise will be a reason to use as small a value as possible consistent with robust stability.

Through much trial and error the parameters used for all simulations were:

$$\varphi = \begin{bmatrix} 1 & 0 & 0 \\ 0 & 10 & 0 \\ 0 & 0 & 10 \end{bmatrix} \tag{III-30}$$

$$\eta = \begin{bmatrix} 1 & 0 & 0 \\ 0 & 10 & 0 \\ 0 & 0 & 10 \end{bmatrix} \tag{III-31}$$

and

$$\lambda = \begin{bmatrix} 0.075 & 0 & 0 \\ 0 & 5 & 0 \\ 0 & 0 & 5 \end{bmatrix} \tag{III-32}$$

The values for φ were selected so that significant errors would be required before saturation developed. The values of η were selected to offset the reduction in the sliding surface function caused by the φ term. Since most operations will occur while $\sigma < 0.4\varphi$ then

$$\eta \frac{\tanh(\sigma)}{\varphi} \cong \sigma \tag{III-33}$$

The values of λ were selected to ensure that heading errors dominated the rudder controls. In this mode rudders will operate in opposite direction for maximum turning rate. As positional errors grow they will mitigate this effect turning the stern rudder as to gain the path thus reducing the turning rate of the vehicle.

D. AUV SIMULATION RESULTS

To validate this MIMO control theory we will generate curved paths using various continuous curvature shapes. Curved paths developed from zero, sinusoidal and sawtooth shaped curvature were generated as commands to track using the control laws developed. These examples will demonstrate that the MIMO control system does provide adequate control in an AUV application.

Figure III-1 illustrates a straight line path represented by the dashed line in the "POSITION" frame. The simulated AUV path is the solid line. The initial position was off the track starting point by 0.1 feet in both the x and y directions. As simulations began the heading errors were small thus the position errors dominate and the controller ordered the bow and stern rudders, DRb and DRs respectively, to work together in the same direction causing the AUV to crab sideways regaining track.

Figure III-2 demonstrates the controllers ability to track a slowly varying sinusoidal curvature with a maximum curvature of $0.0375(ft^{-1})$. In this situation the heading error dominates until heading is nearly matched. The rudders orders are proportionally in opposite directions to establish the turn rate required. As position errors grow they begin to dominate and the stern rudder slowly shifts direction attempting to regain track with lateral force. Notice that the bow rudder follows the curvature shape while the stern rudder compensates for position offset.

The Figure III-3 simulation increases the magnitude of curvature to develop a tight turn. The heading error is large dominating the rudder commands until the rudder limits are reached. This clipping action allows the heading and position errors to grow more rapidly. As the position errors grow they contribute more to the rudder controls shifting the direction of the aft rudder in an attempt to use the sway force to regain the path.

In simulation Figure III-4, with a sawtooth shaped curvature, the effects of the discontinuous curvature rate were tested. The discontinuities did cause transients but had little effect on the performance of the controller.

In Figure III-5, a circle of twenty foot radius was tracked. This constant curvature path allowed the controller to achieve a constant heading and positional error. The x and y position errors are sinusoidal. The sum of there errors are a constant magnitude. The bow and stern rudders achieve a steady state position where the bow rudder generates the turning rate and the stern rudder generates a sway force to hold a constant path offset.

Figure III-6 used the same initial conditions of Figure III-2 but a 0.2 knot current in the x direction was applied. The control system reaches a steady state offset in position to develop the rudder order required to compensate for the current. Also note that the speed order was reduced due to current assisting in the path direction. This figure illustrates the need for integral control to remove the steady state bias. But integral control causes problems in track following. The response from integral control is second order and can be very oscillatory. With any form of integral control, however, care must be taken to avoid the reset windup problem. The current system with its associated errors is " good enough".

POSITION (feet)

OFFSET DISTANCE (feet)

SIGMA

DEL
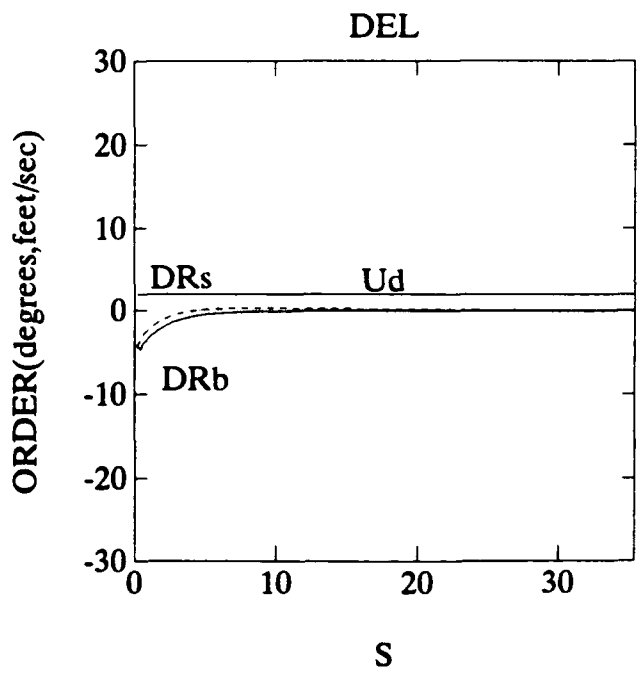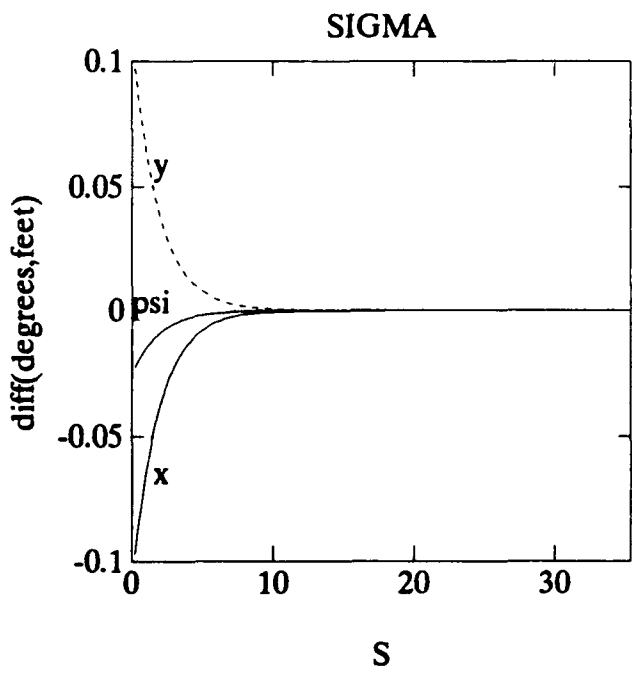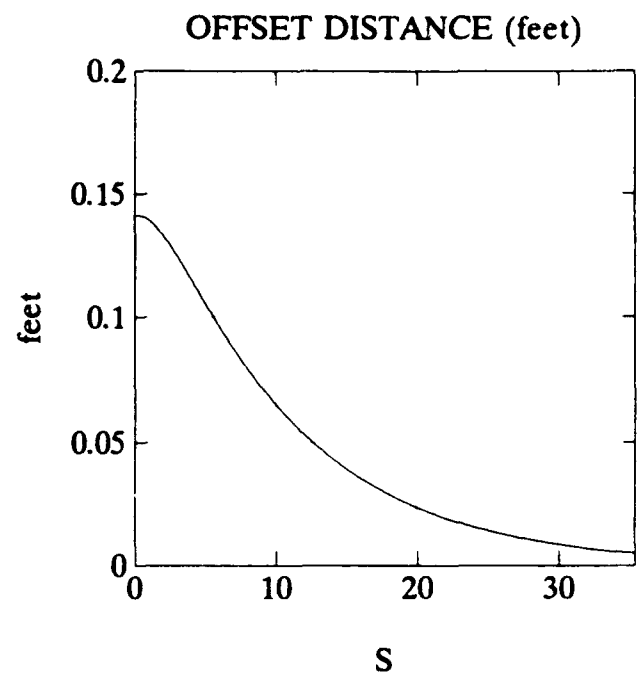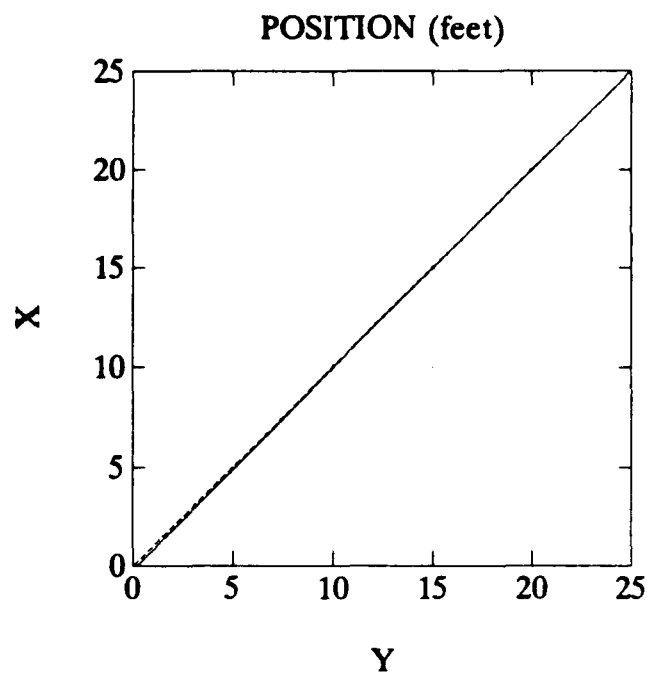
Figure III-1. AUV Simulation Straight Path

24

Curvature and dK/dS

POSITION(feet)

K & dK/dS

0.1

0.05

0

-0.05

-0.1

0   50   100 150 200

S

X

100

50

0

0   50   100

Y

SIGMA

DEL

diff(degrees,feet)

4

2

0

-2

-4

psi

y

x

0   50   100 150 200

S

ORDER(degrees,feet/sec)

30

20

10

0

-10

-20

-30

DRb

Ud

DRs

0   50   100 150 200

S
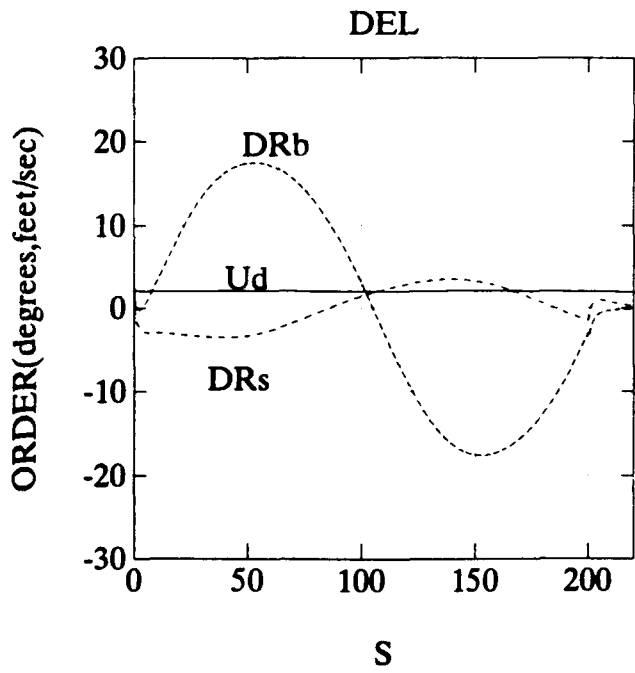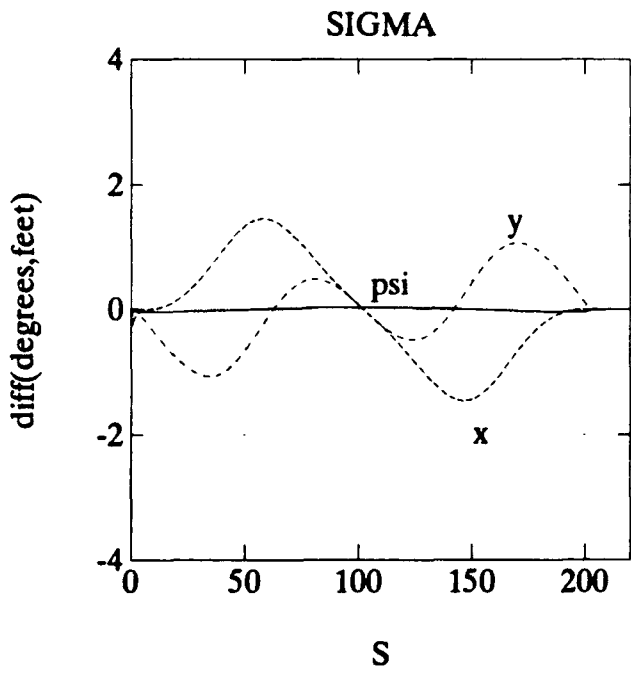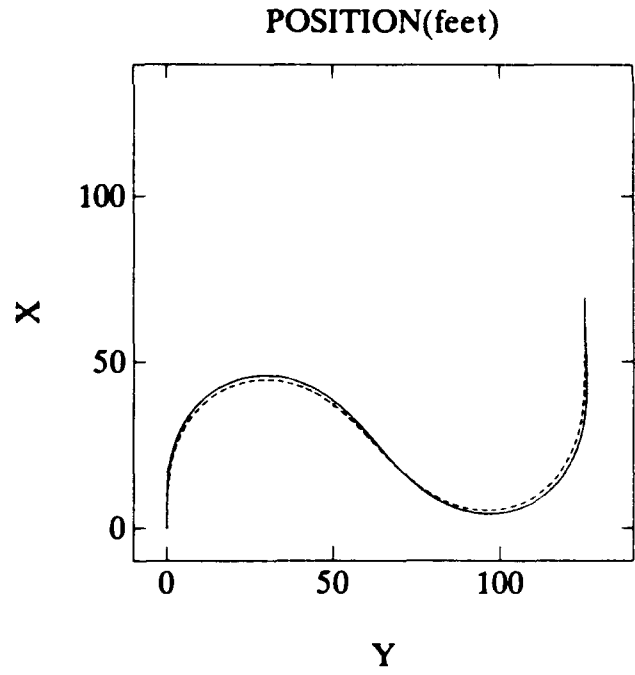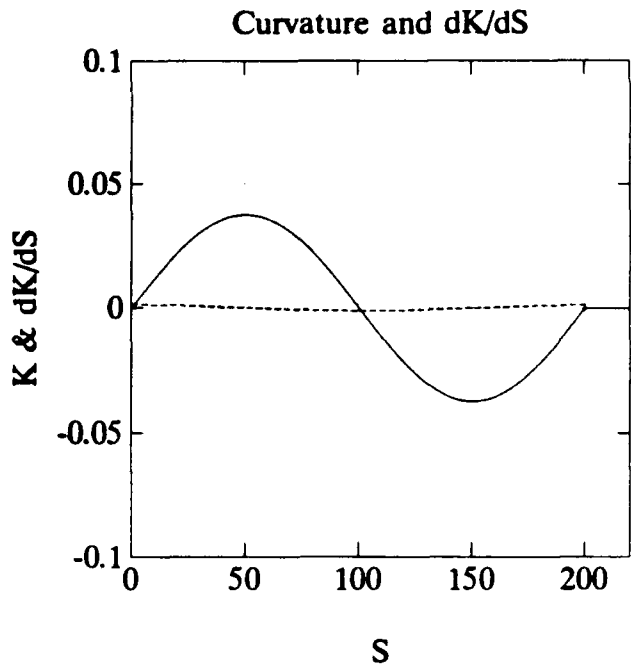
Figure III-2.   AUV Simulation Sinusoidal Curvature (Shallow Turn)

25
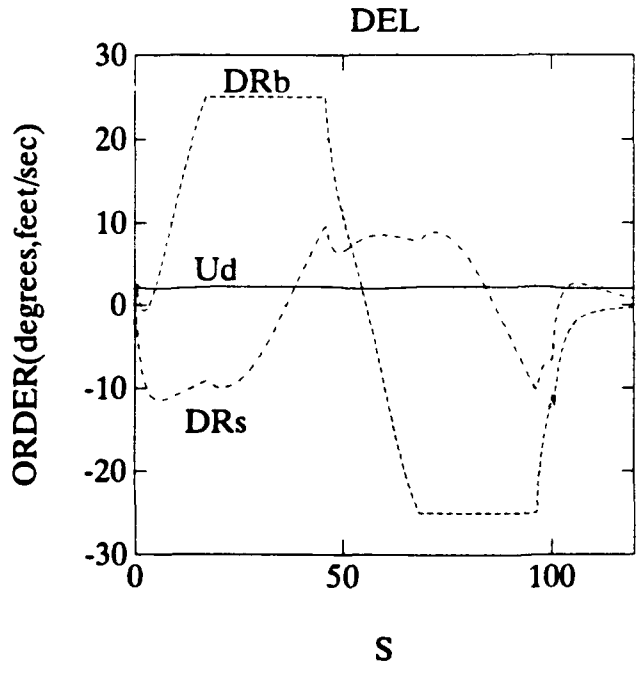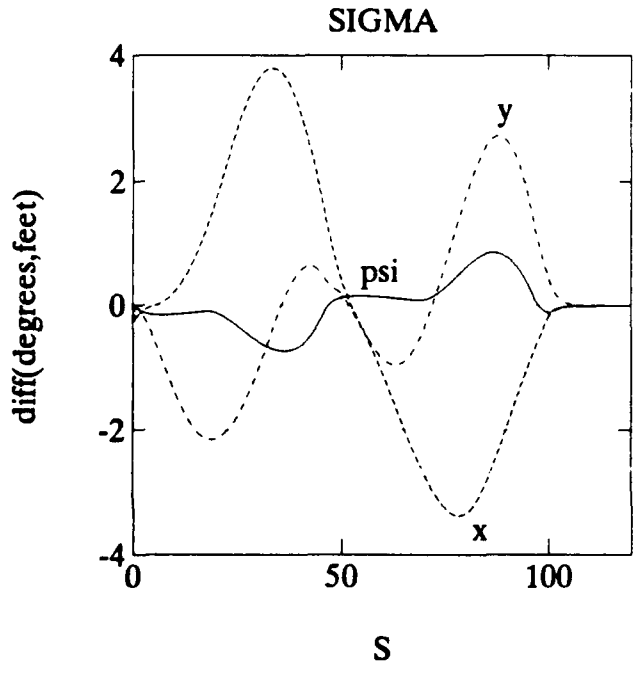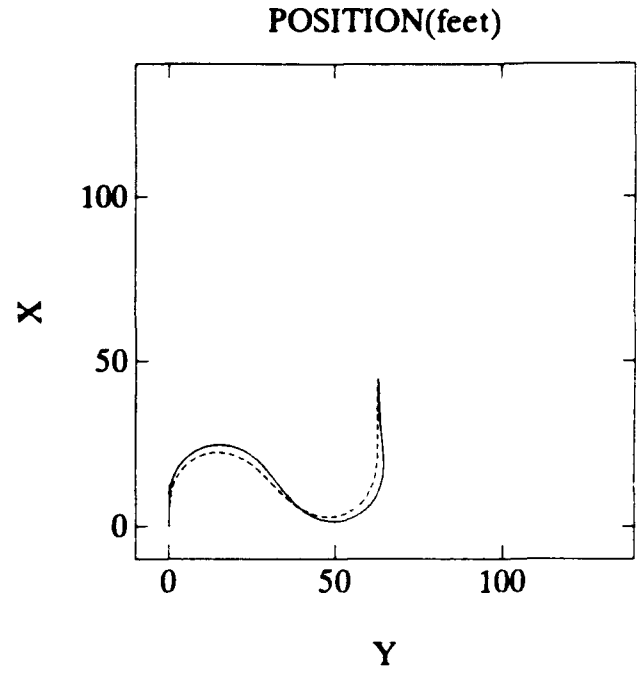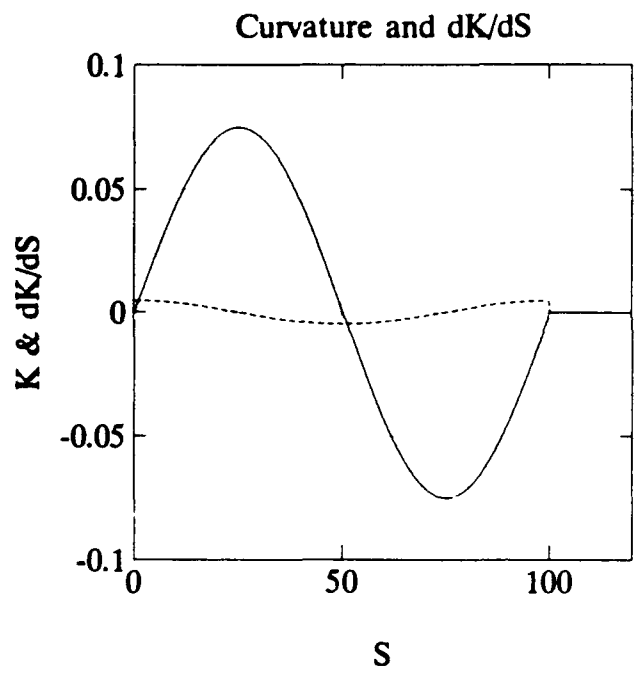
Figure III-3.   AUV Simulation Sinusoidal Curvature (Sharp Turn)
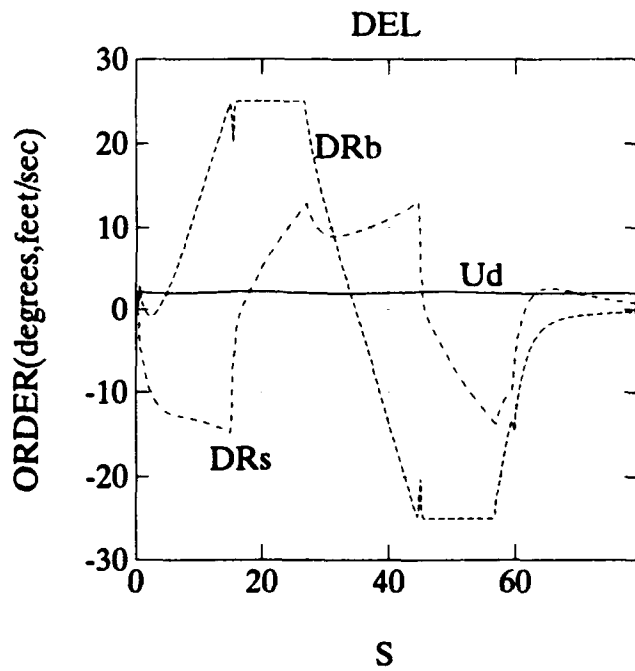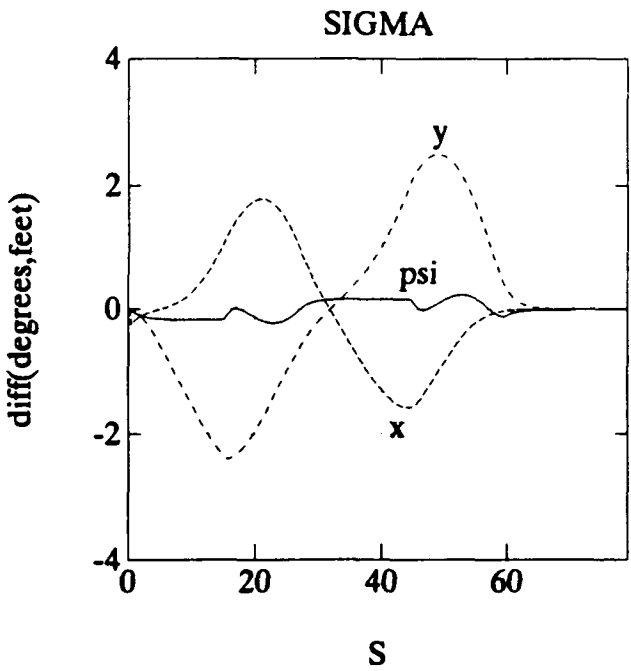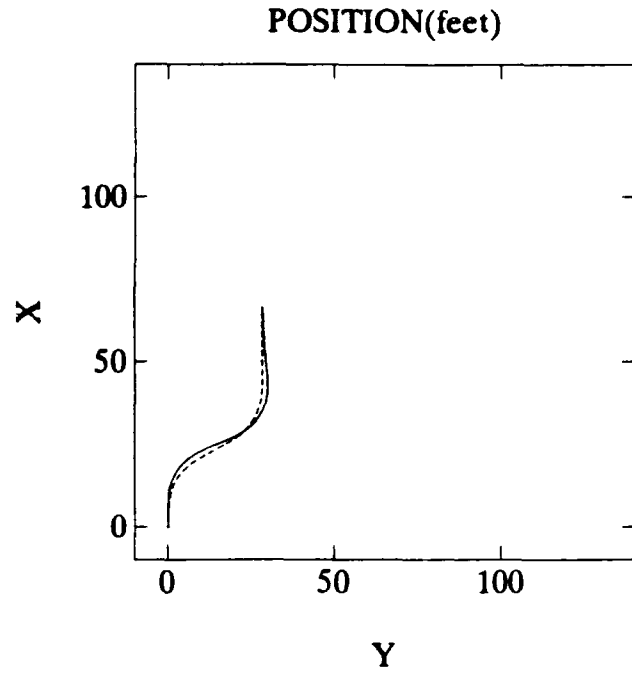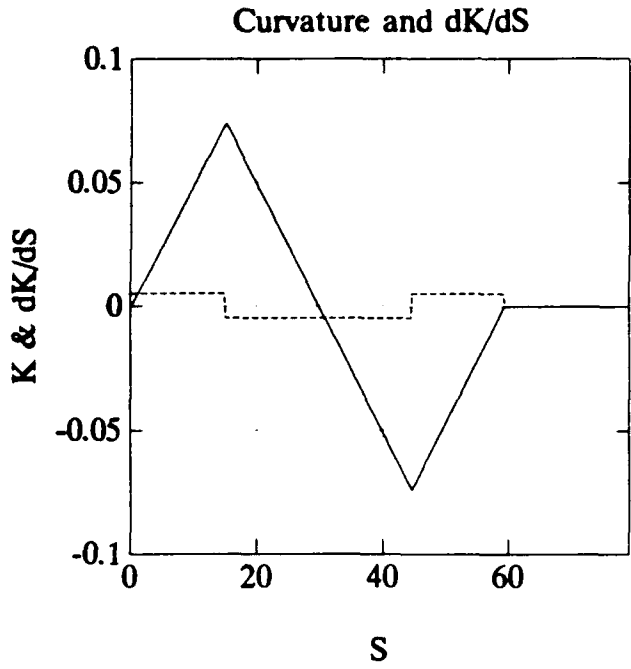
Figure III-4. AUV Simulation Sawtooth Curvature

27
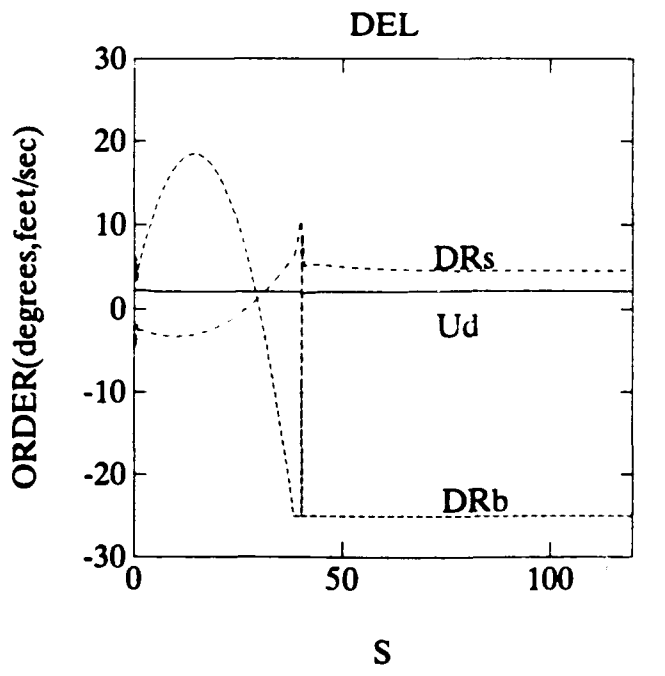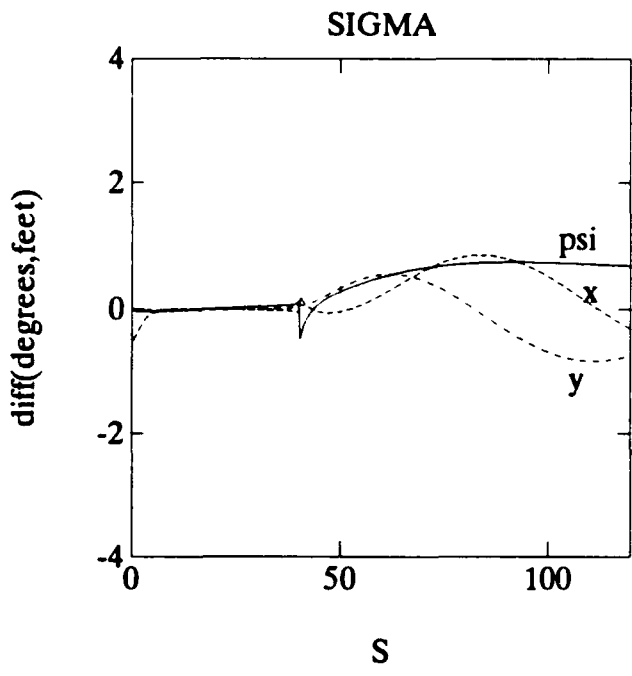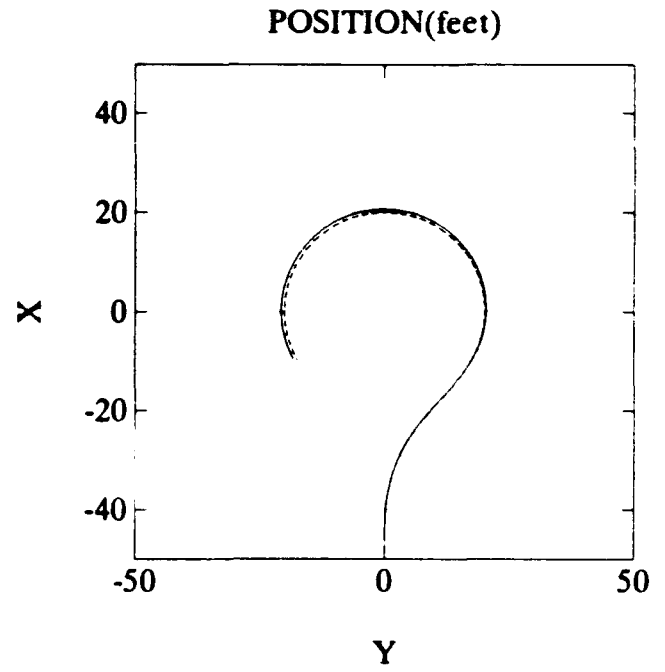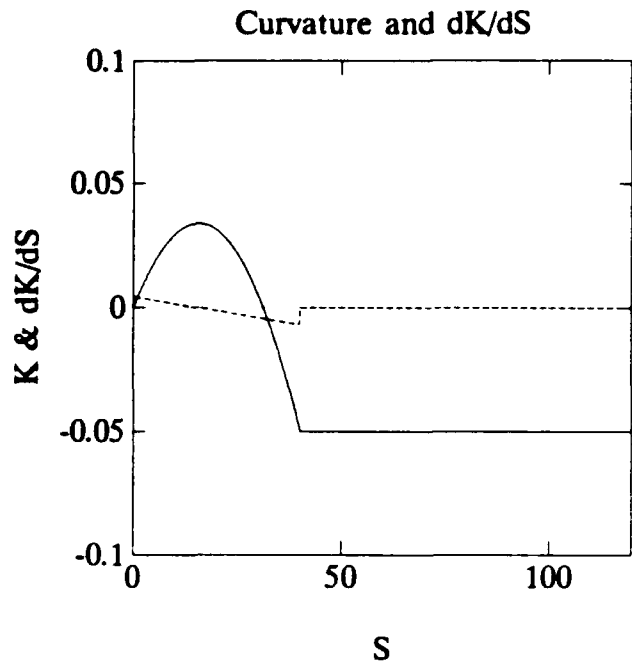
Figure III-5.   AUV Simulation Constant Curvature
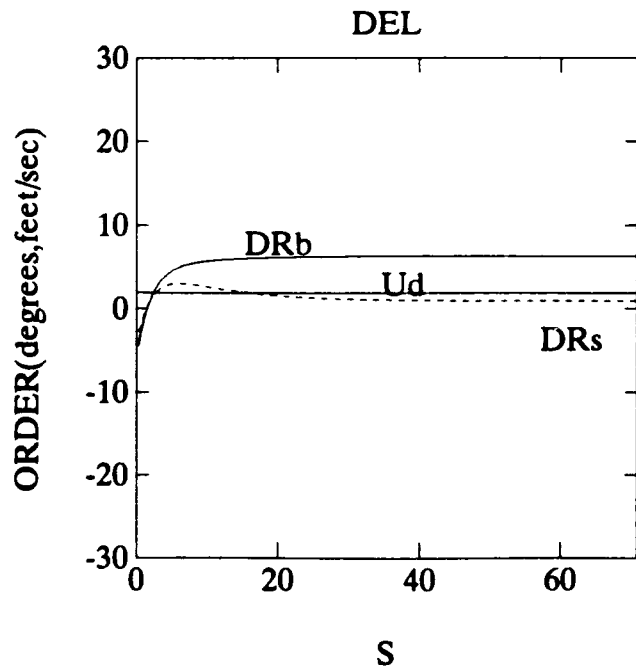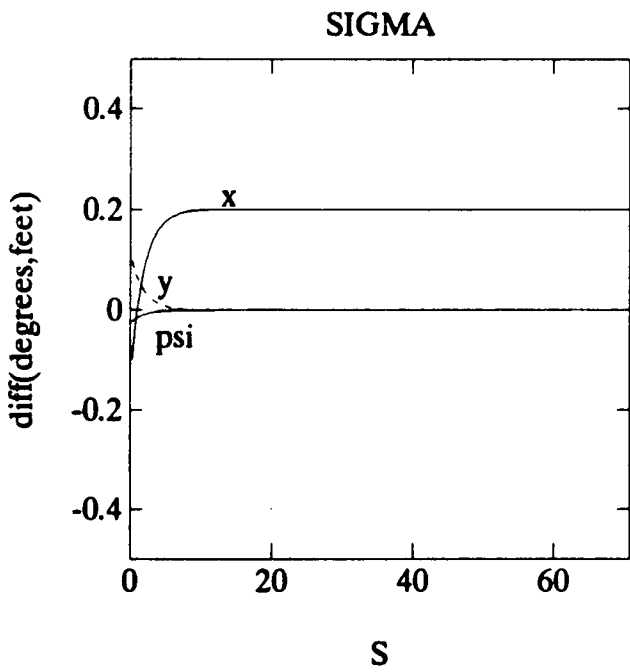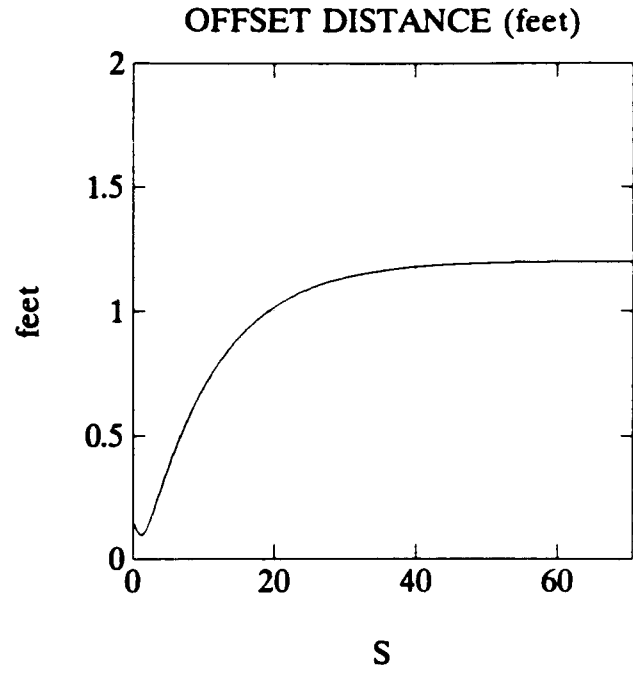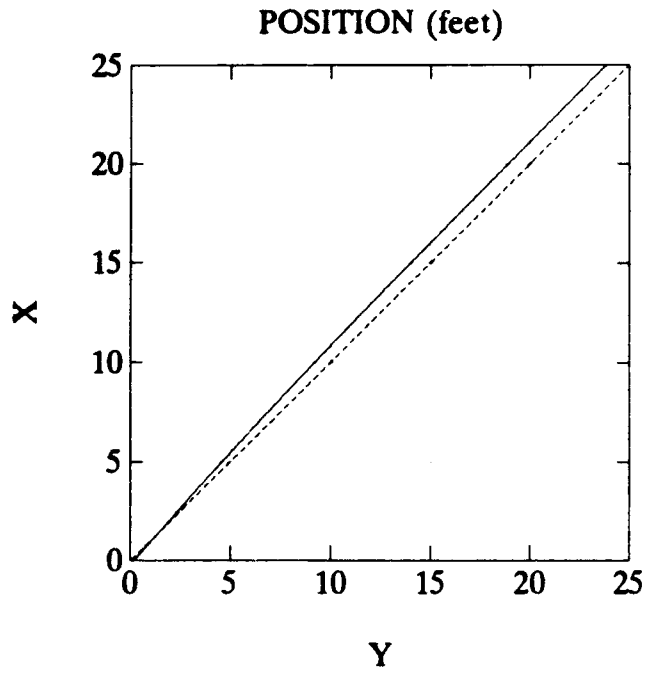
Figure III-6.   AUV Simulation Straight Path with 0.2 Knot Current

IV. GENERATION OF DYNAMICALLY STABLE CURVED PATHS

It has been shown that a nonlinear control system can be designed to drive a submarine vehicle and follow a continuously changing curved path. Now we are interested in developing a path for the vehicle that will inherently follow a directed waypoint track while avoiding objects such as in a mine field. This process consisted of three steps:

1. Develop a waypoint track following algorithm.

2. Develop a sensor model to determine if a mine is within sensor range. Then generate a change in path curvature of sufficient magnitude to avoid the obstacle without exceeding the control capabilities of the vehicle.

3. Incorporate multiple way points in the directed path.

A. PATH KINEMATICS

Consider a path whose incremental change is measurable over a constant time interval Δt. The incremental translational motion is Δs along the path for each data point and its incremental orientation change is $\Delta \Theta$ in each incremental time interval. Therefore:

$$U = \frac{\Delta s}{\Delta t} = \frac{ds}{dt} \quad \rightarrow \quad \Delta s = U \Delta t, \tag{IV-1}$$

and

$$\dot{\Theta} = \frac{\Delta \Theta}{\Delta t} = \frac{d\Theta}{dt} \quad \rightarrow \quad \Delta \Theta = \dot{\Theta} \Delta t. \tag{IV-2}$$

Assume that the path's configuration is $q(s)=f(x(s),y(s),\Theta(s))$ at s and the incremental values of Δs and $\Delta \Theta$ are given for the next time interval. Knowing this we can "DEAD RECKON" the path by Euler integration. The next orientation can be determined by:

30

$$x(s + \Delta s) = x(s) + \Delta s \cdot \cos(\Theta(s) + \Delta\Theta / 2)$$

$$y(s + \Delta s) = y(s) + \Delta s \cdot \sin(\Theta(s) + \Delta\Theta / 2).$$ (IV-3)

$$\Theta(s + \Delta s) = \Theta(s) + \Delta\Theta$$

Thus the next configuration is:

$$q(s + \Delta s) = (x(s + \Delta s), y(s + \Delta s), \Theta(s + \Delta s)).$$ (IV-4)

By approximating this curve as a circular arc with an average curvature, the radius of curvature then becomes:

$$r = \frac{\Delta s}{\Delta\Theta} = \frac{U}{\dot\Theta} \quad \text{if} \quad \Delta\Theta \neq 0.$$ (IV-5)

The path curvature (K) is defined as the inverse of the radius of curvature and can be expressed in terms of the yaw rate and path speed as:

$$K = \frac{1}{r} = \frac{\Delta\Theta}{\Delta s} = \frac{\dot\Theta}{U} \quad \text{if} \quad \Delta\Theta \neq 0.$$ (IV-6)

Figure IV-1 illustrates the geometry of the path. If we evaluate the length of the straight line segment (d) over the time interval Δt then:

$$\frac{d/2}{r} = \sin\left(\frac{\Delta\Theta}{2}\right).$$ (IV-7)

Solving for d:

$$d = 2r \cdot \sin\left(\frac{\Delta\Theta}{2}\right).$$ (IV-8)

We can now rewrite the kinematic equations:

$$x(s + \Delta s) = x(s) + d \cdot \cos(\Theta(s) + \Delta\Theta / 2)$$

$$y(s + \Delta s) = y(s) + d \cdot \sin(\Theta(s) + \Delta\Theta / 2).$$ (IV-9)

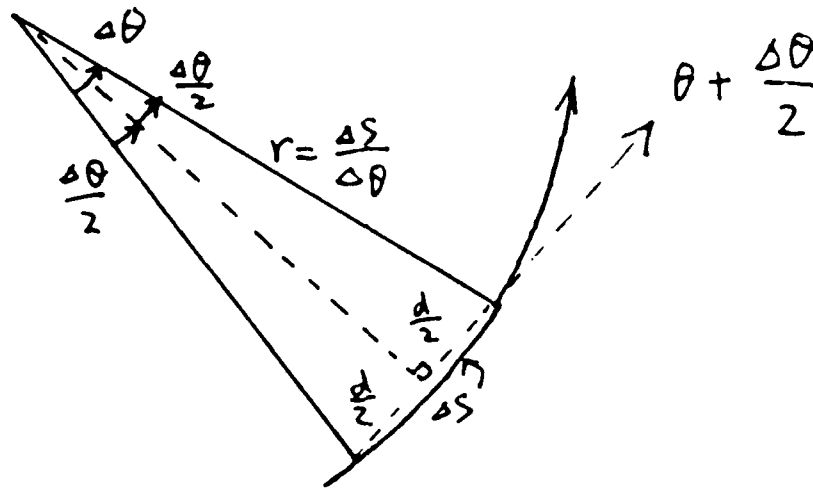$$\Theta(s + \Delta s) = \Theta(s) + \Delta\Theta$$

Figure IV-1. Path Geometry

B. PATH GENERATION

Stable paths may be generated if path curvature is controlled. In particular, a path may be generated and forced to regain some desired path defined by $q = f(K_{im}, \Theta_{im}, x_{im}, y_{im})$ if $(D, \Delta K, \Delta \Theta) \to 0$ as $t \to \infty$ where D is the perpendicular distance from the current orientation to the desired path and

$$\Delta K = (K - K_{im})$$ (IV-10)

and

$$\Delta \Theta = (\Theta - \Theta_{im}).$$ (IV-11)

Then curvature can be controlled by a specification for dK/ds, which we call the "Steering Function", to be a continuous function of the path variables. This would ensure K is continuous and smooth.

32

$$\frac{dK}{ds} = f(q, P, S) \tag{IV-12}$$

ΔK, $\Delta \Theta$, and D can be forced to go to zero by the stable path control given by:

$$\frac{dK}{ds} = -(a \cdot \Delta K + b \cdot \Delta \Theta + c \cdot D). \tag{IV-13}$$

Since $K = \dfrac{d\Theta}{ds}$ and $\Delta \Theta \cong \dfrac{dD}{ds}$ for small errors in heading. The differential equation can be reduced to

$$D''' + aD'' + bD' + cD = 0$$

$$(\rho^3 + a\rho^2 + b\rho + c)D = 0 \tag{IV-14}$$

$$(\rho + k)^3 D = 0$$

where a, b, and c are positive constants.

$$a = 3k$$
$$b = 3k^2 \qquad \text{where } k \text{ is a constant.} \tag{IV-15}$$
$$c = k^3$$

Then the solution to this equation is of the form

$$D = f(s)e^{-ks} \tag{IV-16}$$

where $D \to 0$ as $s \to \infty$.[Ref. 8]

This then reduces the steering function from a three degree of freedom function to a single degree of freedom, and k^{-1} becomes a characteristic length. This single variable k adjusts the sensitivity of the control to give rapid or gentle return to the directed track and ensures a stable result. As k becomes smaller the path is less responsive reaching the directed track more slowly. As k becomes larger the path more rapidly acquires the directed track.

Once dK/ds is calculated, it is used to change the current path curvature (K) to merge with the directed track. Thus using Euler integration of the path kinetics, K is:

$$K(i) = K(i-1) + (dK/ds) \cdot \Delta s, \tag{IV-17}$$

33

where Δs is the incremental path length. The change in the orientation ($\Delta \Theta$) associated with this change in curvature can be calculated:

$$\Delta \Theta = K(i) \cdot \Delta s \qquad \text{(IV-18)}$$

Using Equation (IV-9), the next path position can be calculated with this orientation change and the incremental path length. Changing these equations to the discrete time domain we get:

$$x(i+1) = x(i) + U(i) \cdot \cos(\Theta(i) + \dot{\Theta}(i)dt/2)dt$$

$$y(i+1) = y(i) + U(i) \cdot \sin(\Theta(i) + \dot{\Theta}(i)dt/2)dt \, . \qquad \text{(IV-19)}$$

$$\Theta(i+1) = \Theta(i) + \dot{\Theta}(i)dt$$

This process progresses through the entire path length. This algorithm was tested with orientations and tracks in every quadrant to ensure validity. Since the nonlinear controller also needs commanded velocity and acceleration terms to define the feed forward terms, we get

$$\dot{x}(i) = U(i) \cdot \cos(\Theta(i) + \dot{\Theta}(i)dt/2)$$

$$\dot{y}(i) = U(i) \cdot \sin(\Theta(i) + \dot{\Theta}(i)dt/2) \qquad \text{(IV-20)}$$

$$\dot{\Theta}(i) = U(i)K(i)$$

and using a Eularian approximation:

$$\ddot{x}(i) = \frac{\dot{x}(i) - \dot{x}(i-1)}{dt}$$

$$\ddot{y}(i) = \frac{\dot{y}(i) - \dot{y}(i-1)}{dt} \qquad \qquad \text{(IV-21)}$$

$$\ddot{\Theta}(i) = U(i)\frac{dK(i)}{dt} + \dot{U}(i)K(i) = U^2(i)\frac{dK(i)}{ds} + \dot{U}(i)K(i)$$

This is a discrete approximation and will give errors if rapid or discontinuous changes in K take place.

34

The continuous curvature path has many uses. It can be used to redirect vehicle motion and response characteristics when off track to regain the desired path. It allows the control designer to direct a path to follow during transition from one track segment to another at waypoints. Finally, the primary purpose of this thesis, it allows easy integration for reflexive path generation in obstacle avoidance.

C. OBSTACLE AVOIDANCE PATH GENERATION

Now that we have developed a stable path to follow the desired path, we must address the problem of avoiding any obstacles along the way. The goal is to achieve smooth transition from track following to an avoidance mode so that $d\kappa/ds$ generates continuous curvature. If a rule based switch is used for transition, discontinuities would be introduced in $d\kappa/ds$. This "jerk" must be minimized to ensure a continuous curvature. A smooth transition into avoidance could be obtained if $d\kappa/ds$ for avoidance ($del\kappa_a$) were developed from environmental information and summed with the path following term ($del\kappa_p$) as discussed previously. This would provide a total $d\kappa/ds$ for path generation.

$$\frac{d\kappa}{ds} = del\kappa_p + del\kappa_a \qquad (IV-22)$$

For a smooth transition into avoidance the $del\kappa_a$ term should be zero at the initial detection of an obstacle and grow as the range to the obstacle decreases. For smooth transition back to path following $d\kappa/ds$ should return to zero while passing the closest point of approach (CPA). This occurs when the relative bearing (BRG) to the mine is $\pm 90°$. Thus $d\kappa/ds$ will be a function of a range term ($del\kappa_r$) and a relative bearing term ($del\kappa_b$). To provide control of the rate of avoidance a scaling term (K_{scale}) is needed. The product of these terms will give smooth transition into and out of obstacle avoidance.

$$del\kappa_a = del\kappa_r \cdot del\kappa_b \cdot K_{scale} \qquad (IV-23)$$

35

There were many iterations in the functions used for these terms. The equation providing the best transition characteristics was.

$$delK_a = \left(\frac{Rh_{sensor} - Rh_{min}}{Rh_{min} - Rh_{avoid}}\right) \cdot \left(1 - \frac{abs(BRG)}{\pi/2}\right) \cdot \left(\frac{abs(BRG)}{BRG}\right) \cdot K_{scale} \qquad (IV-24)$$

During path tracking, at a ten hertz update rate, obstacles detected within the sensor range, (Rh_{sensor}) set at fifty feet, are considered for avoidance. For vehicle safety a minimum avoidance range (Rh_{avoid}) was set at twenty feet. To keep Rh_{avoid} from being violated the amount of dK/ds would need to be grow significantly as the vehicle approaches close to Rh_{avoid}. This could be achieved if $delK_r$ was inversely proportional to the range to the mine (Rh_{min}) minus Rh_{avoid}. Using this equation, as Rh_{min} crosses into sensor range the $delK_r$ term is zero but as it approaches Rh_{avoid} the term approaches infinity. This provides a smooth application of dK/ds while preventing the violation of Rh_{avoid}. As BRG approaches $\pi/2$ the $delK_b$ term reduces to zero. Thus at the closest point of approach (CPA) the value of dK/ds for avoidance is zero. At the same time, Rh_{min} is increasing and the control mode shifts back to path following.

Several simulations, illustrated in Figures IV-2 thru IV-5, were run demonstrating the ability to develop a path through the mine field without violating the avoidance range. These paths have curvatures well within the capabilities of the AUV II to negotiate. The maximum curvature required in these cases was about $0.07(\text{ft}^{-1})$. If the avoidance range were reduced the maximum curvature would increase. If reduced too far it would be beyond the capability of the vehicle to follow. A closer avoidance range is impractical for a mine avoidance role.

As the mine field density increases so does the value of dK/ds required to successfully traverse the mine field. These rapid changes in curvature are due to shifting in

36

and out of the avoidance criteria in close proximity to CPA while close to the avoidance range.

D. MINE LOCALIZATION

Showing that a path can be successfully generated in real time through a mine field has many uses besides the obvious passage through. AUVs are being considered for mine localization in a Mine Warfare scenario. By combining a multisegment tracking ability and a search plan along with this avoidance routine, the AUV can be used. A multisegment path transition was accomplished by using a "waypoint reached" criterion. This criterion checks the distance to the next way point in each iteration. It determines a new speed to reach the waypoint on time and if the distance meets the "waypoint reached" criterion, the next waypoint path parameters are calculated and used for calculating the steering function to merge with the new desired path. Combining this with the avoidance routine, paths were successfully generated through several mine field configurations. Figures IV-6 and IV-7 are illustrations of localization and avoidance behaviors of the path generation algorithm for uniformly distributed random mine fields of twenty mines.

E. RESULTS

Using the obstacle avoidance path provides excellent control of the vehicle in even a dense mine field when all detected mines are used to form the avoidance calculation. This tool together with the mission planners directed track provides a safe path through a hostile environment. But as has been seen the change in curvature and the rate of its change is significant in the denser mine fields. There is a possibility that as the avoidance range for adjacent mines overlap, the path may attempt to bisect the mines. The higher density fields are unrealistic in the mine localization role but were used more to illustrate the abilities of the algorithm. The actual vehicle is not capable of dealing with the rapid

changes in curvature generated by some paths. The AUV II has a limit on its rate of change of curvature and maximum curvature. By design then, we must limit curvatures in the specified avoidance track to lie within the bounds of its capabilities.
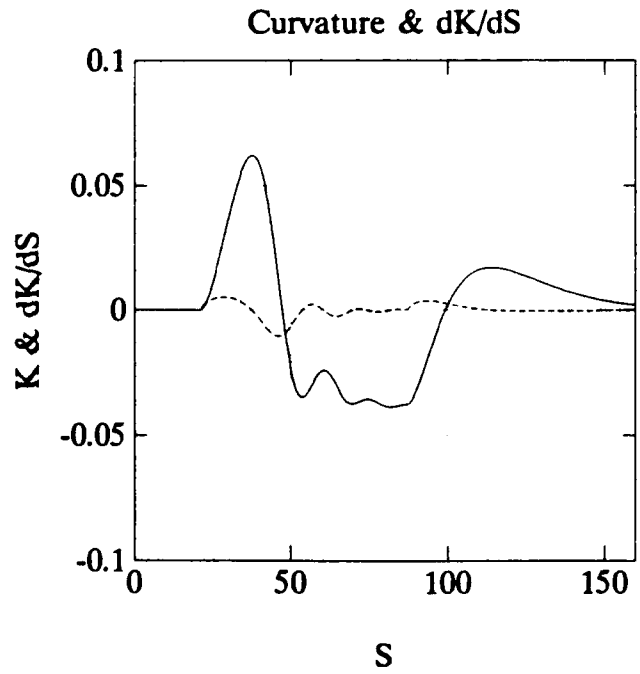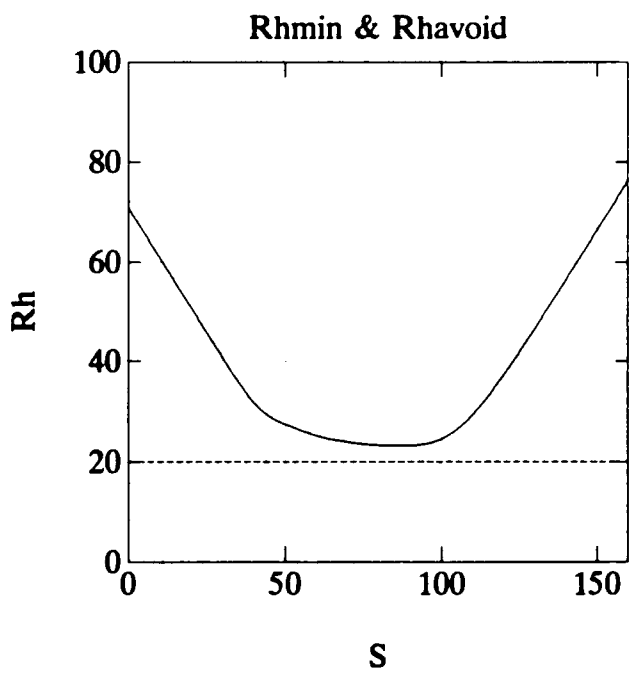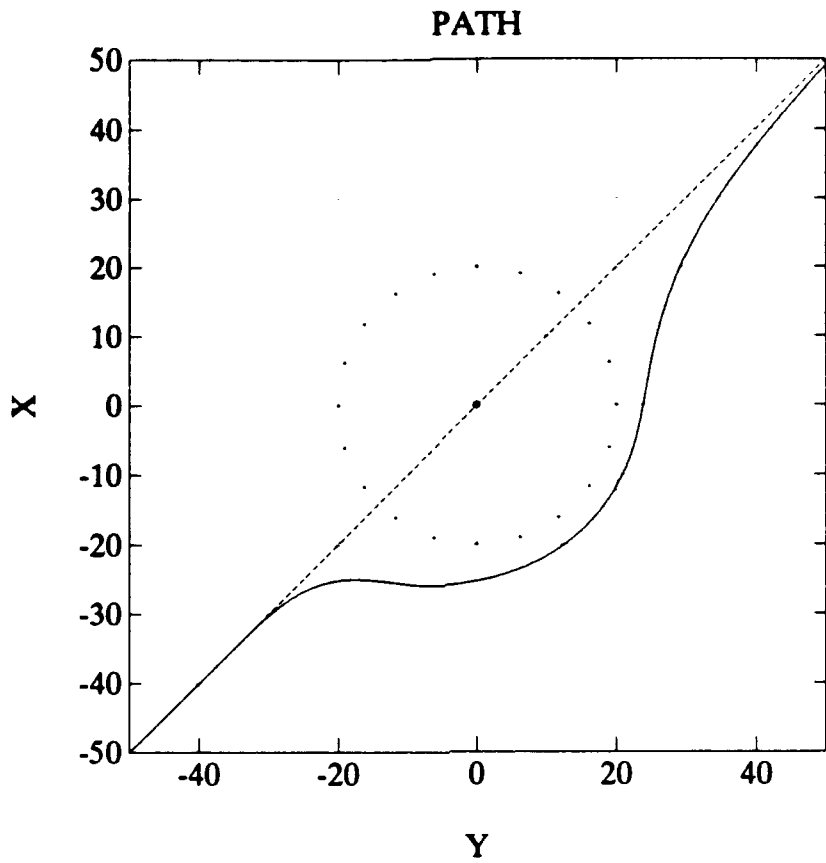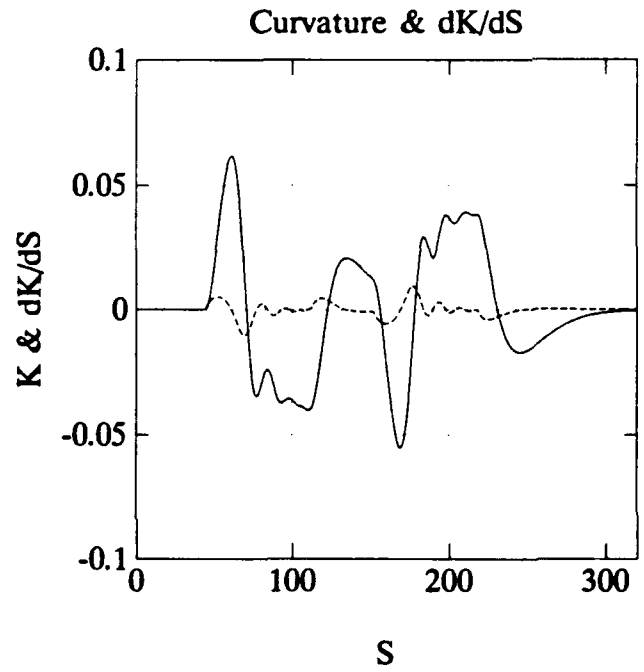
Figure IV-2.   Obstacle Avoidance Single Mine
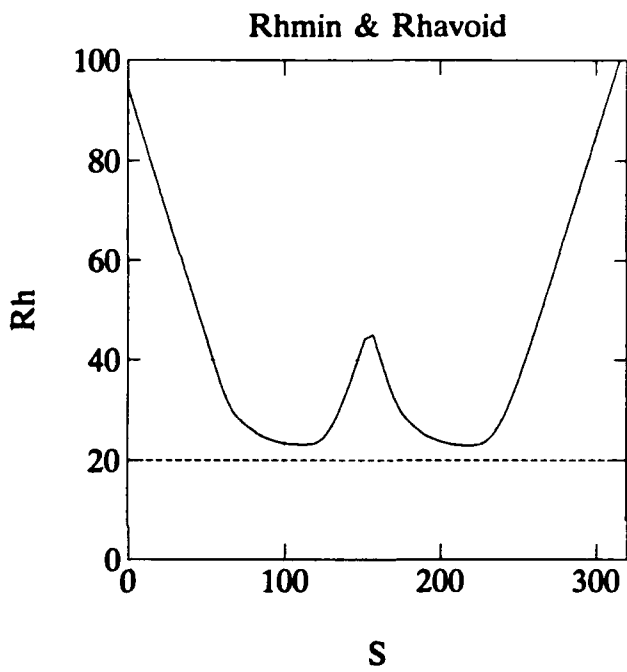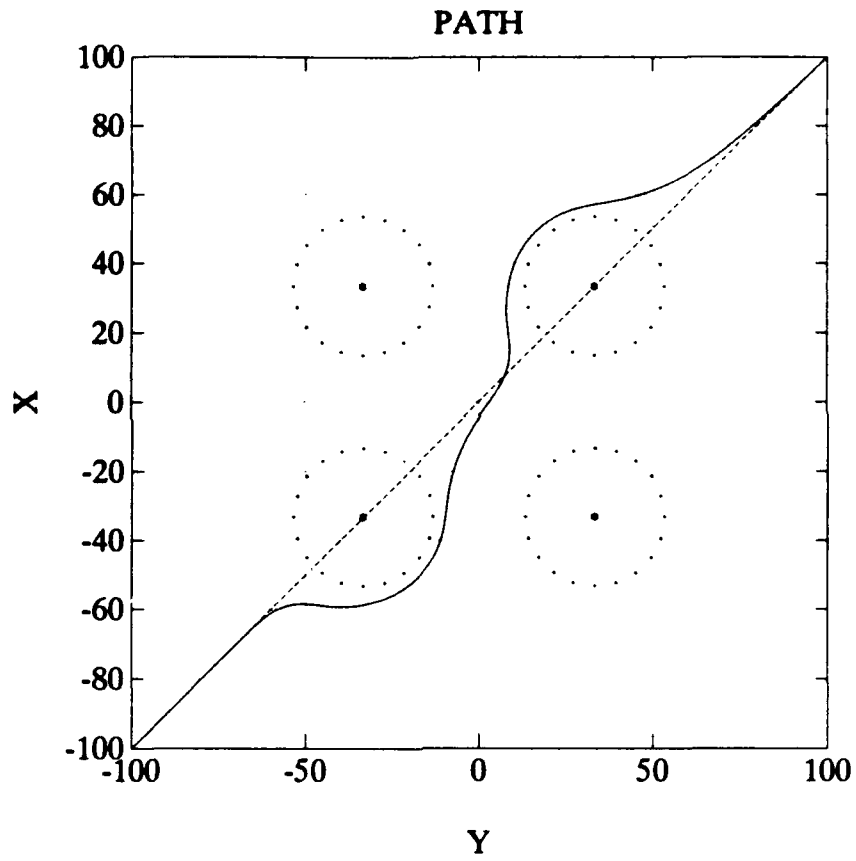
39

PATH

Rhmin & Rhavoid

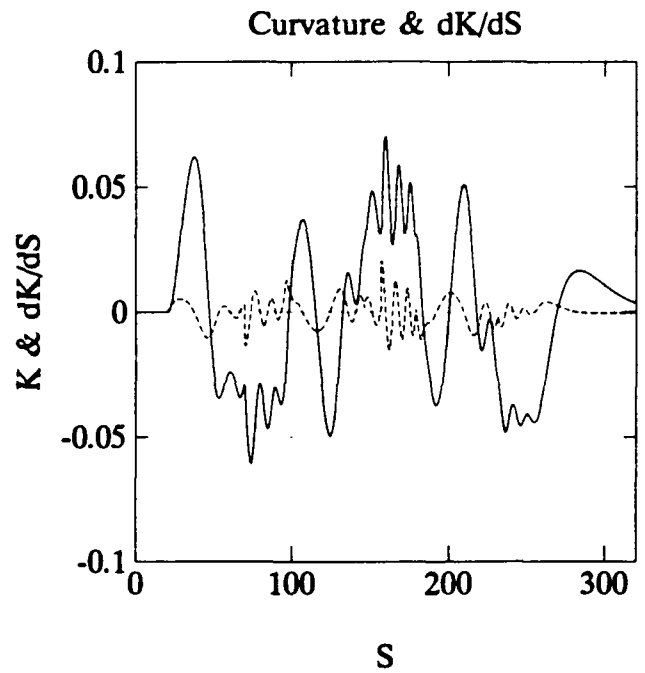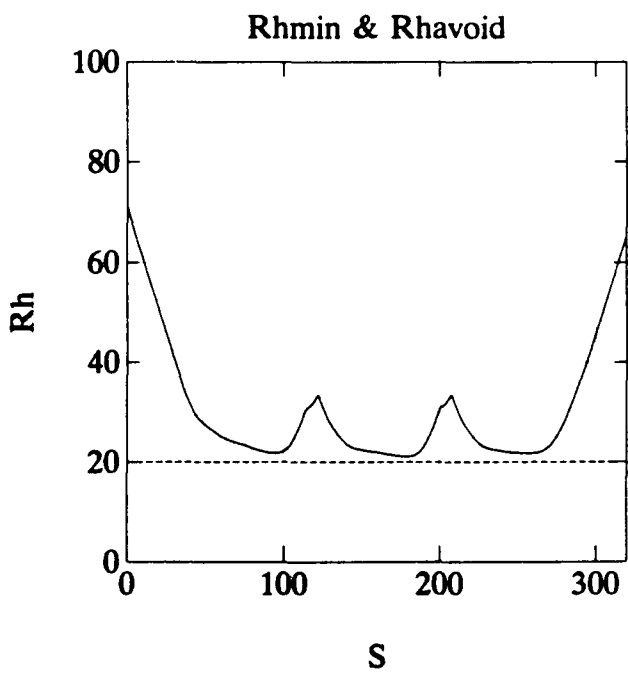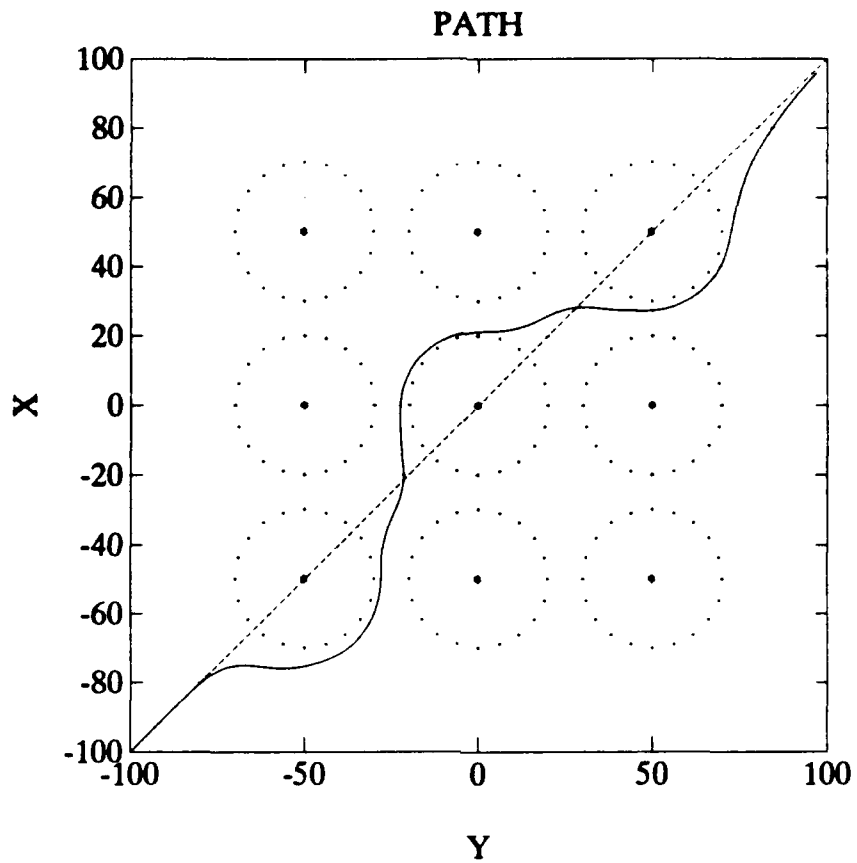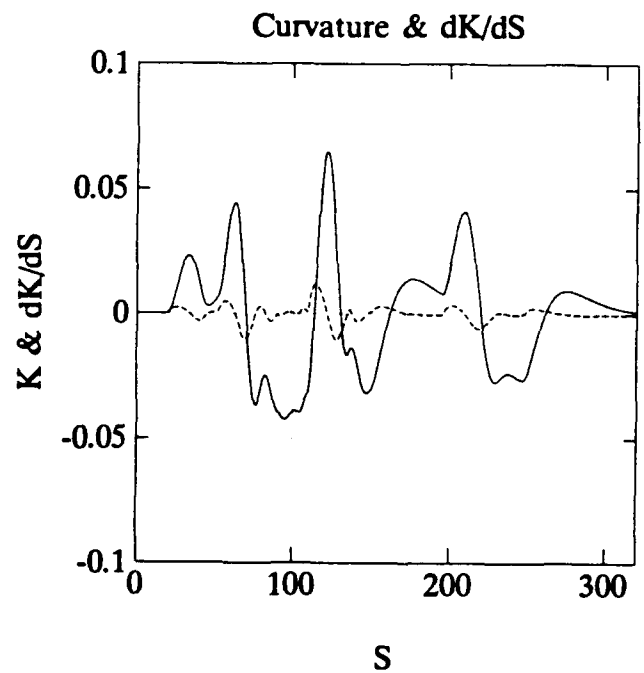## Curvature & dK/dS

Figure IV-3. Obstacle Avoidance Four Equally Spaced Mines

40

PATH

Rhmin & Rhavoid

Curvature & dK/dS

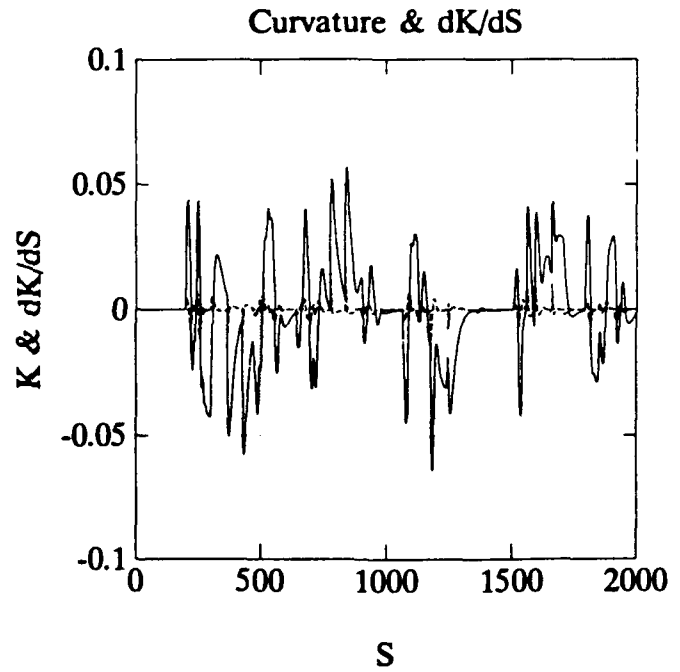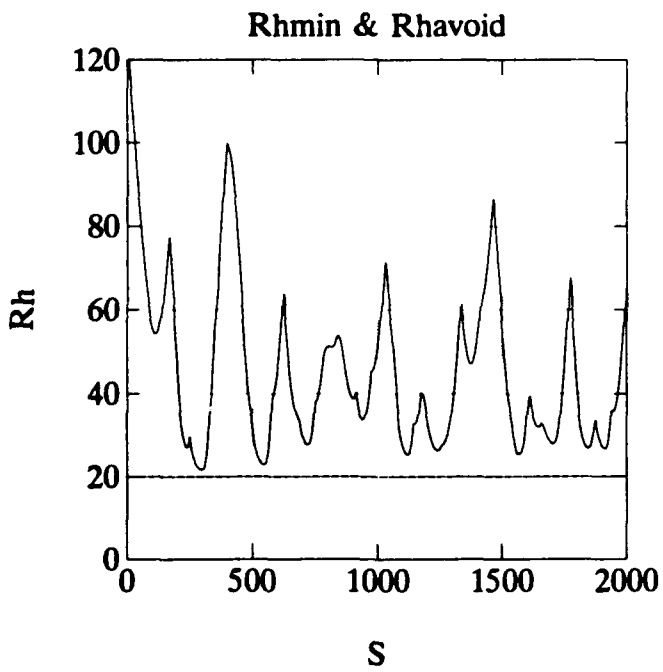Figure IV-4.   Obstacle Avoidance Nine Equally Spaced Mines

41
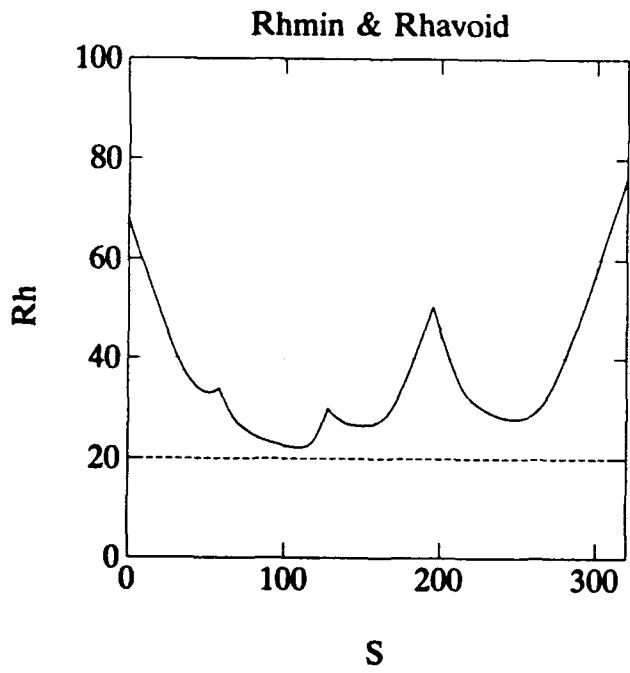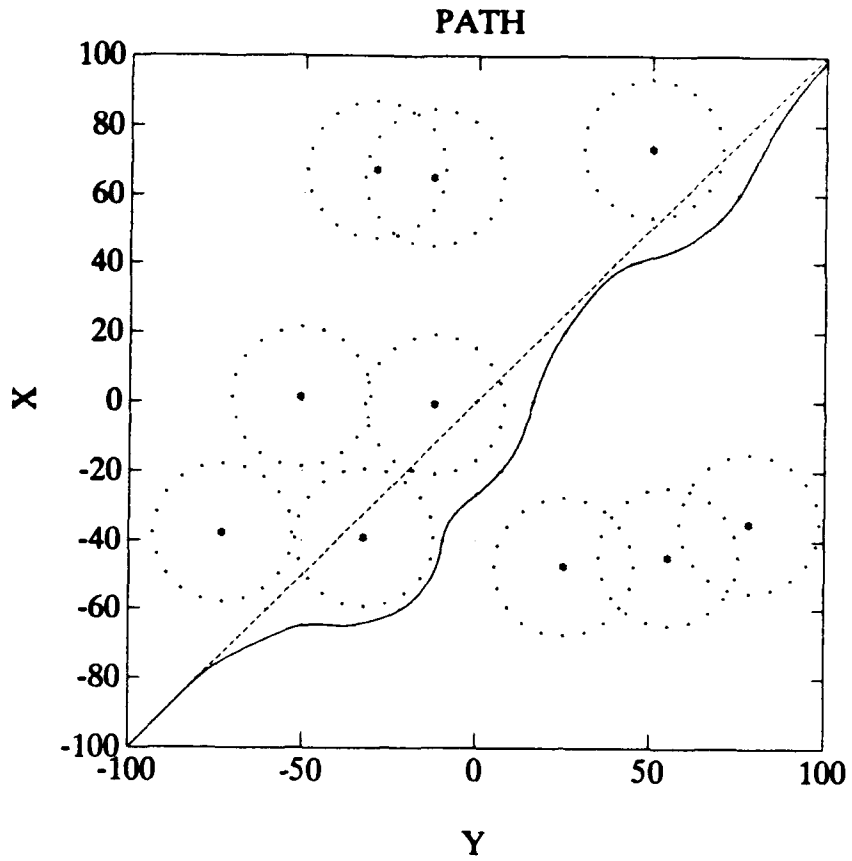
Figure IV-5.   Obstacle Avoidance Ten Randomly Spaced Mines

42

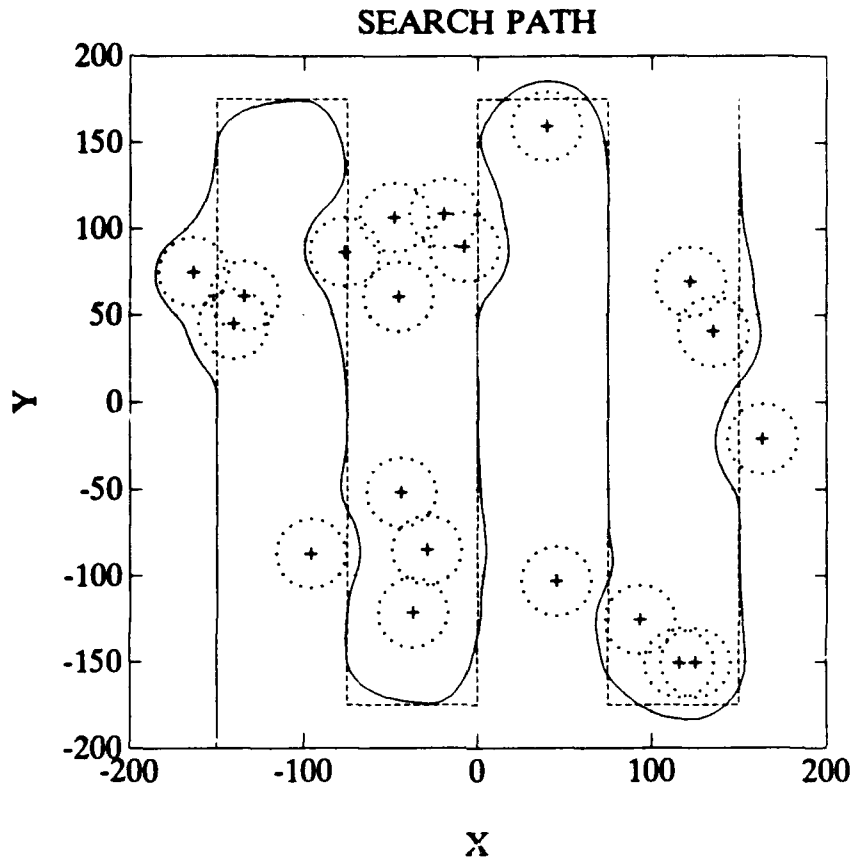Figure IV-6. Mine Localization

SEARCH PATH

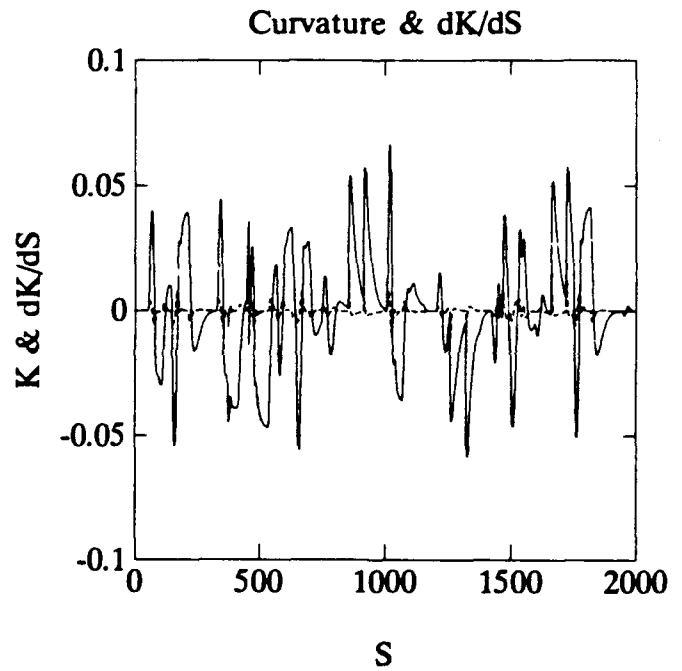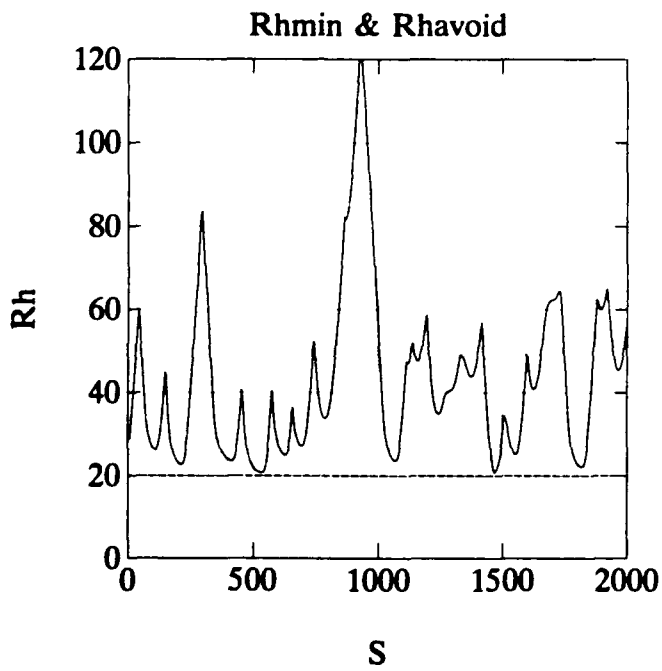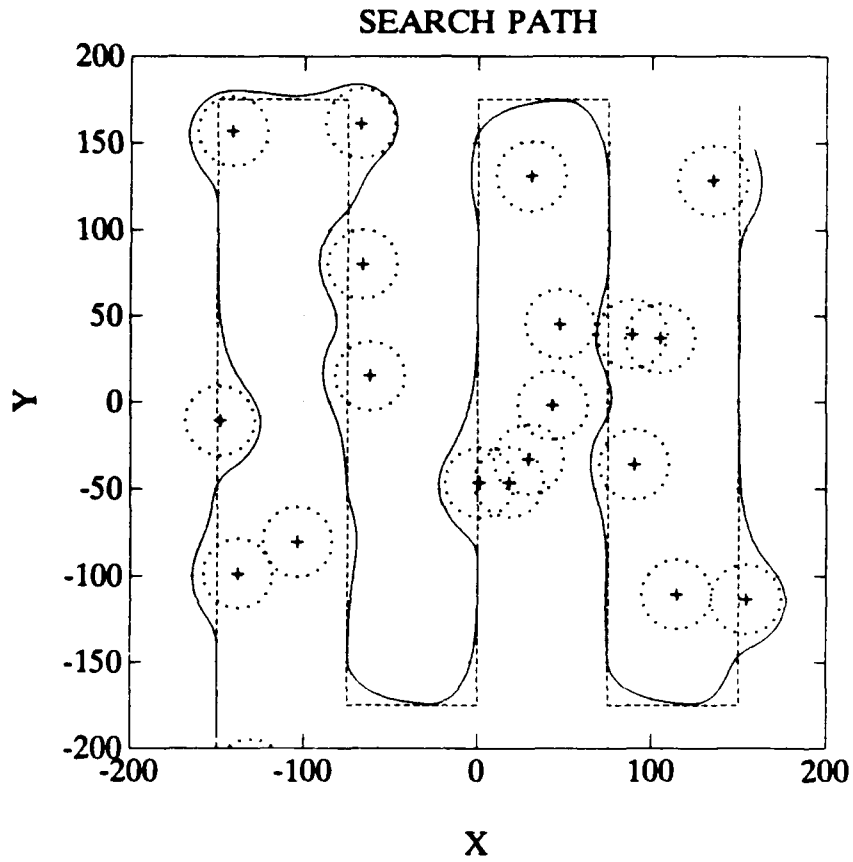## Rhmin & Rhavoid

Curvature & dK/dS

Figure IV-7.   Mine Localization

V. AUV SIMULATION USING PATH GENERATION

We have shown that curvature path control can successfully negotiate a mine field and that the AUV MIMO control system can follow continuous curved paths. But we must realize that we must not create a curved path beyond the capability of the AUV to negotiate. To determine the limits of the AUVs maneuverability a simulation was run with the bow and stern rudders at their limits, 25 degrees. They were positioned in opposite directions to maximize the turning rate. Figure V-1 shows that the maximum curvature in this maneuver is about 0.16 (ft^{-1}) which corresponds to a tactical diameter of about 12.5 feet. The critical parameter for maneuverability is the rate of curvature change. dK/ds must not change too rapidly or the AUV will not be able to develop the turning rate required to maintain the path. If the turning rate is too large heading and position errors will develop. If allowed to grow unchecked these could cause instability of the system. This limiting of dK/ds and curvature terms may prevent successful passage through the higher density mine fields where higher values are required.

To evaluate the combined control system of the AUV several simulations were run. The first simulation positioned a single mine on the desired path. Figure V-2 shows the curvature required to maneuver around the obstacle. This generated the avoidance path depicted in the POSITION plot as the dashed line. The simulated AUV path is depicted as the solid line. The mine is shown as the star with the avoidance range dotted around the mine. The control system lags the avoidance path slightly but position errors do not exceed half a boat length. This "loose" control will allow more uncertainty errors without adversely affecting the performance.

The next simulation, Figure V-3, increased the mine field density. Four mines are arranged around the path. In this case, the avoidance command generator only sees one or two mines at a time. There is plenty of room to maneuver the AUV between the mines before the next mine's avoidance command builds to a point that it dominates the control order.

Increasing the mine density again. Nine mines are positioned equally spaced about the path. In Figure V-4 we see that the increased rate of curvature does generate rapid rudder orders. The rate of rudder change is acceptable.

In the last case, ten randomly distributed mines, were uniformly distributed around the desired path. In a random distribution, the average distance between mines is increased over the equally spaced mine distribution. This provides windows of opportunity for the AUV to pass through which it would not have with an equally spaced mine field of the same density.

Three general observations were made in these simulations. First, rudder clipping at 25 degrees does not allow adequate turning rates required by the controller. This allows positional errors to grow causing the stern rudder to shift in an attempt to force its way back to track. In doing this, positional errors grow even larger. If the path had not reduced its curvature at this point allowing the vehicle to regain track, both rudders would have saturated and control would have been lost. This oscillatory path is very forgiving allowing vehicles to regain track once errors grow. Secondly, the bow rudder order angle is directly proportional to path curvature. This may allow the use of curvature to command the rudders together in an avoidance and path following mode. And thirdly, the positional errors, while turning rapidly around an object, fall outside the path around the mine. Thus the path errors are safely conservative.
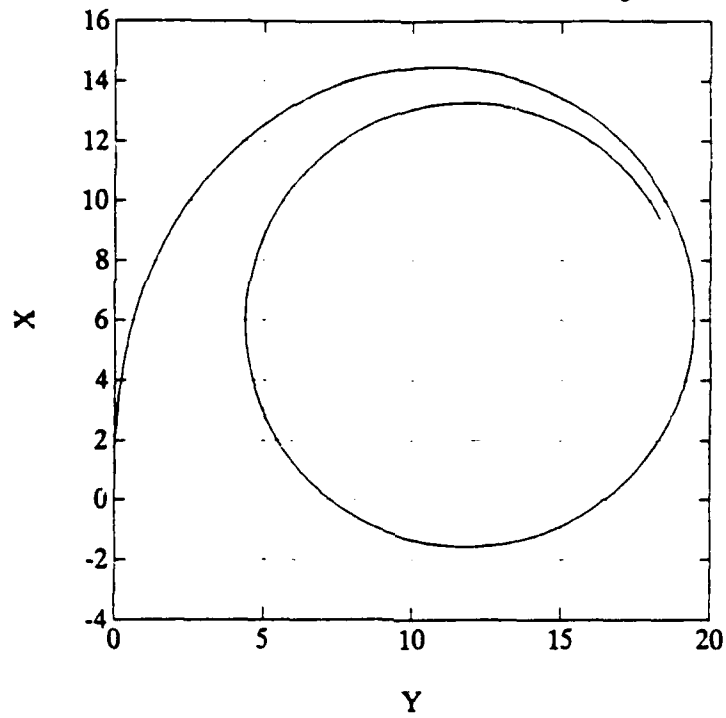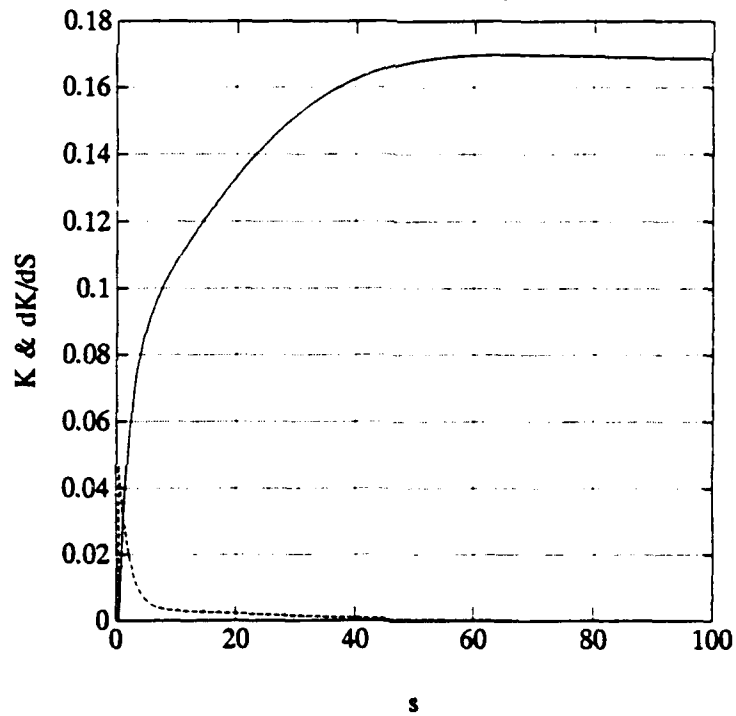
Figure V-1.   AUV Maximum Maneuverability

47
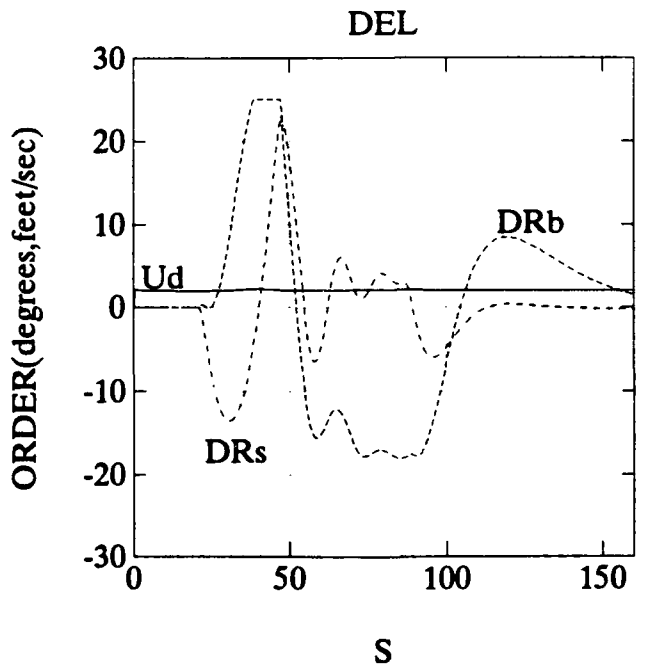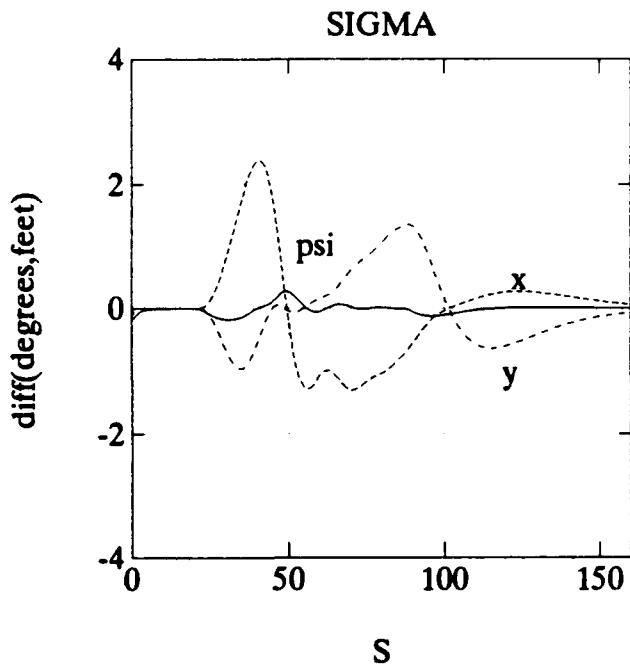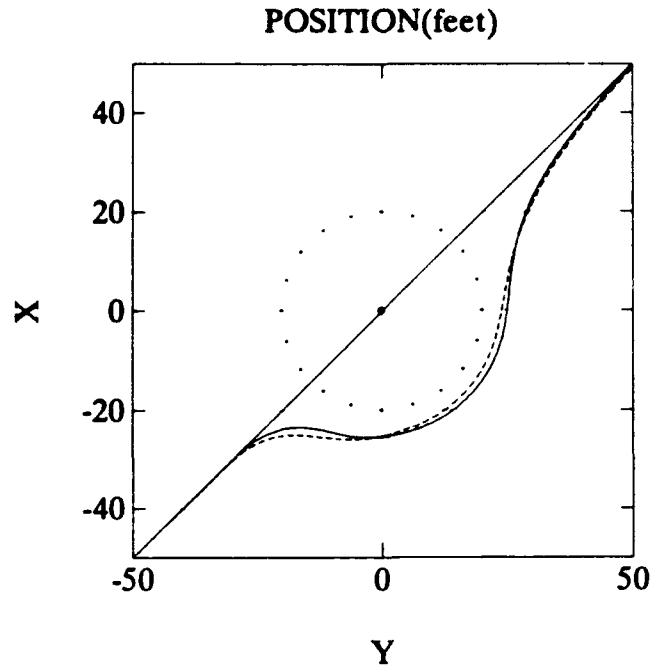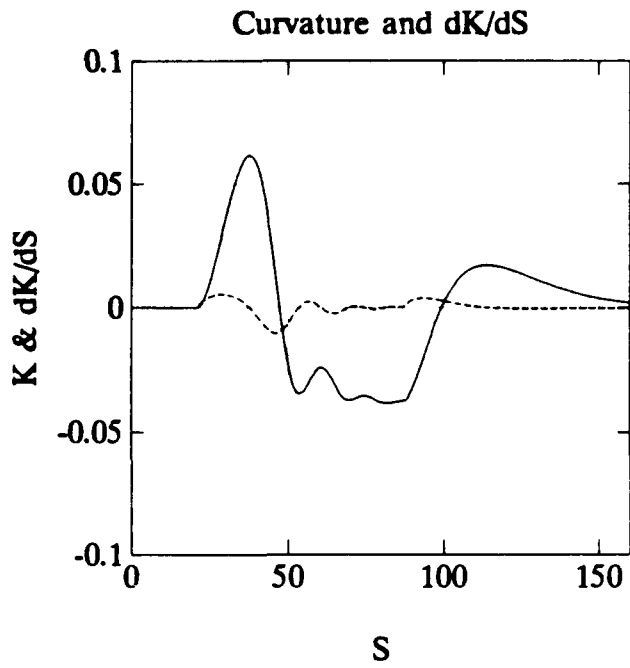
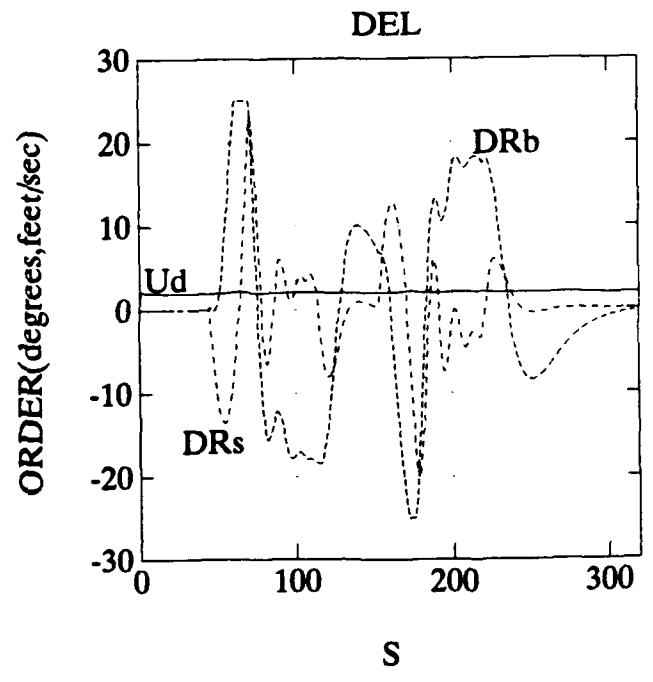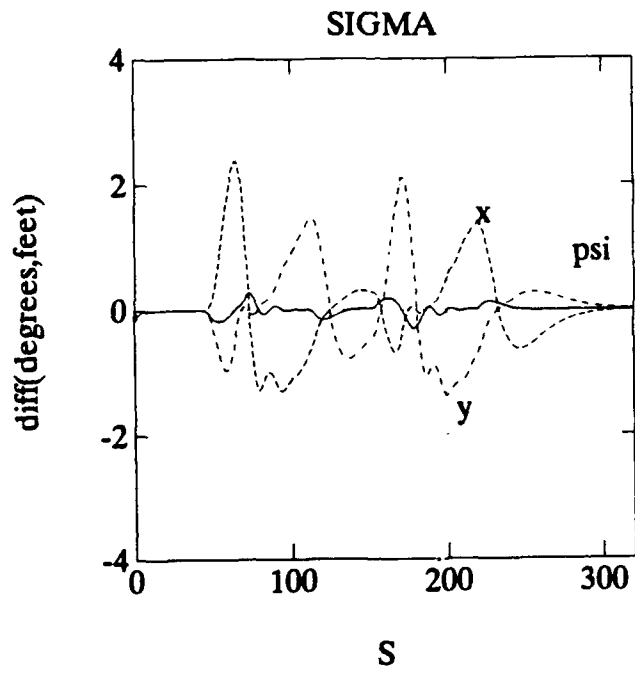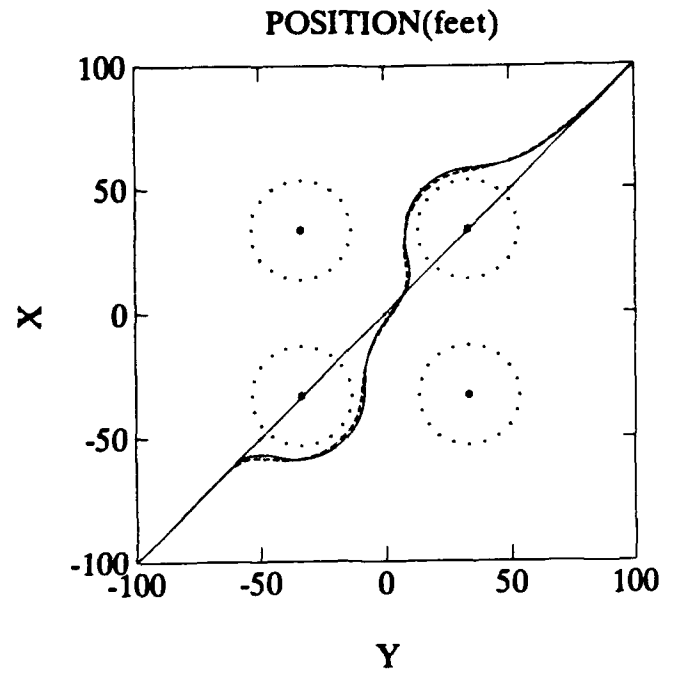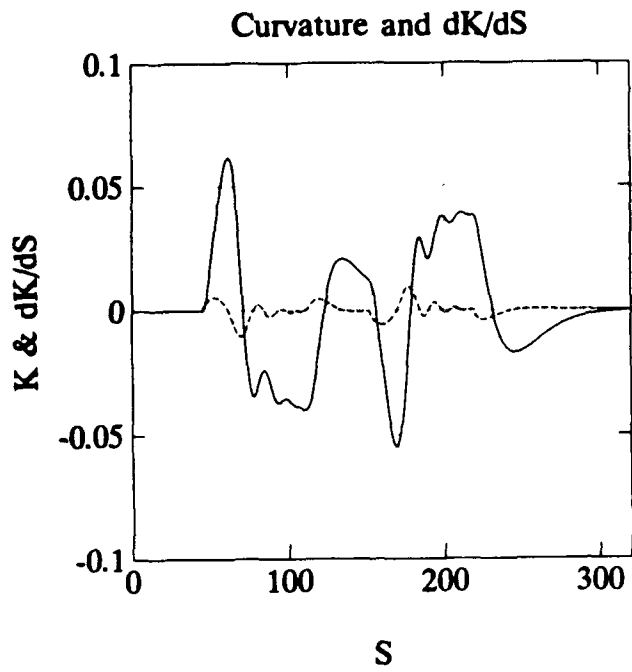Figure V-2.   AUV Simulation: Obstacle Avoidance Single Mine

Figure V-3.   AUV Simulation: Obstacle Avoidance Four Equally Spaced Mines
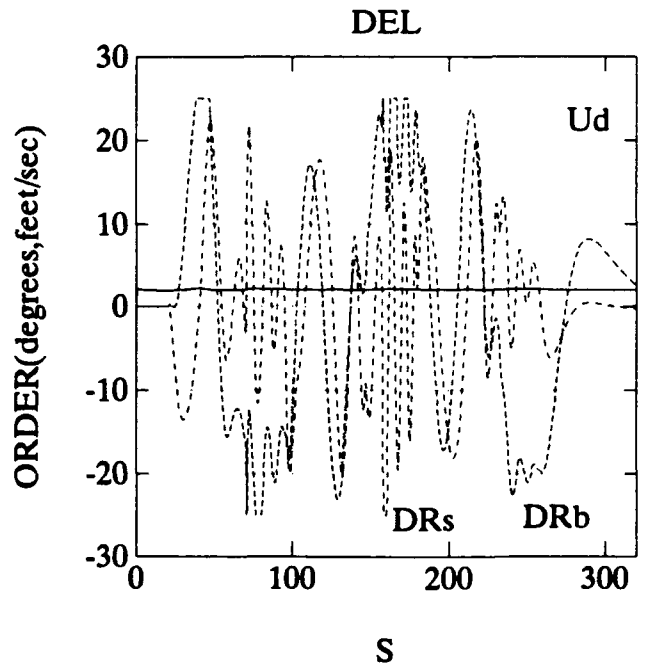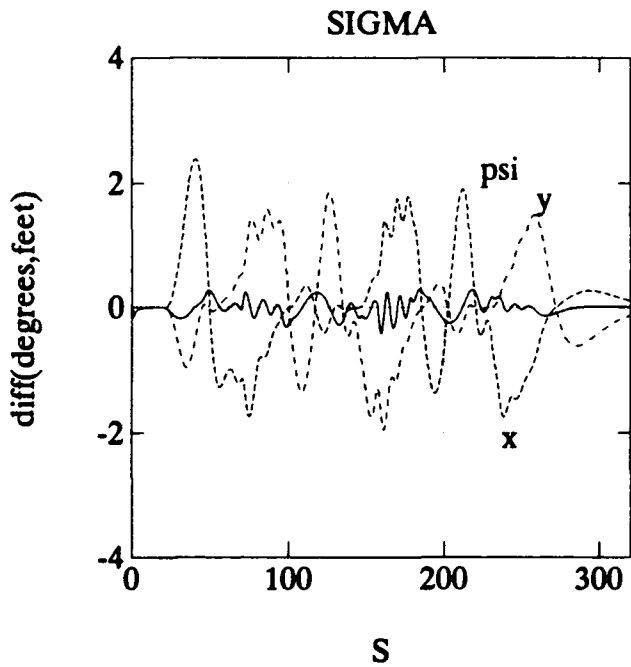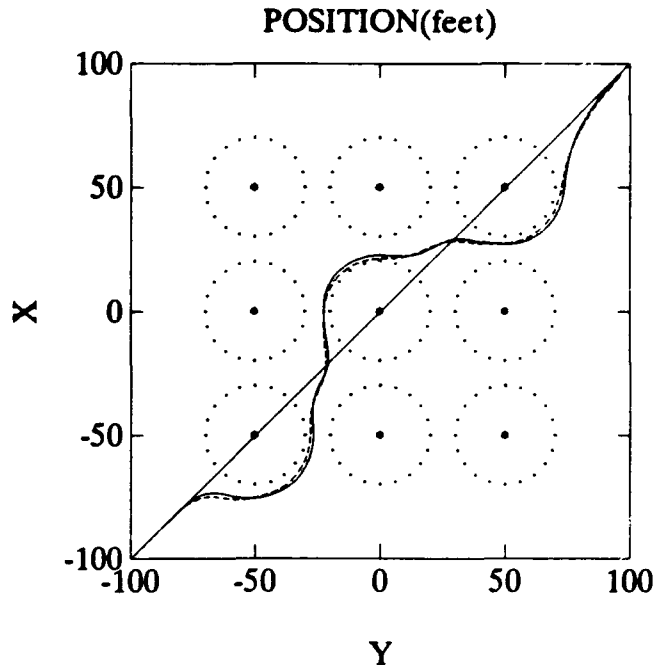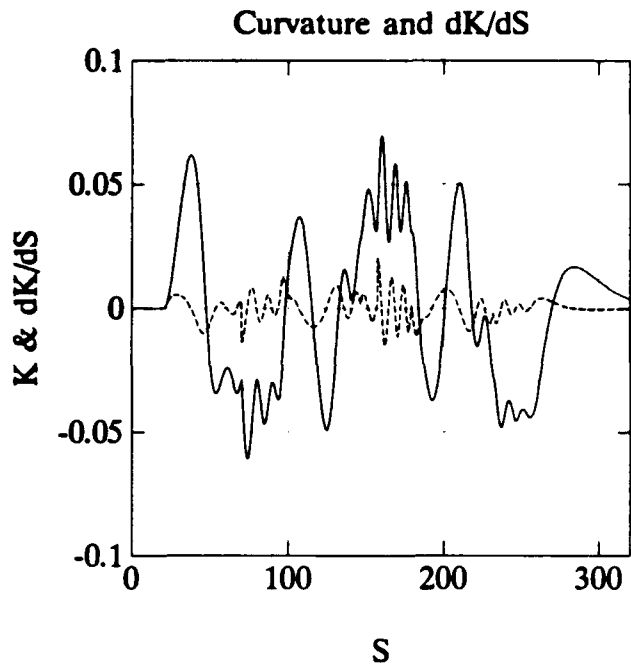
Figure V-4.   AUV Simulation: Obstacle Avoidance Nine Equally Spaced Mines
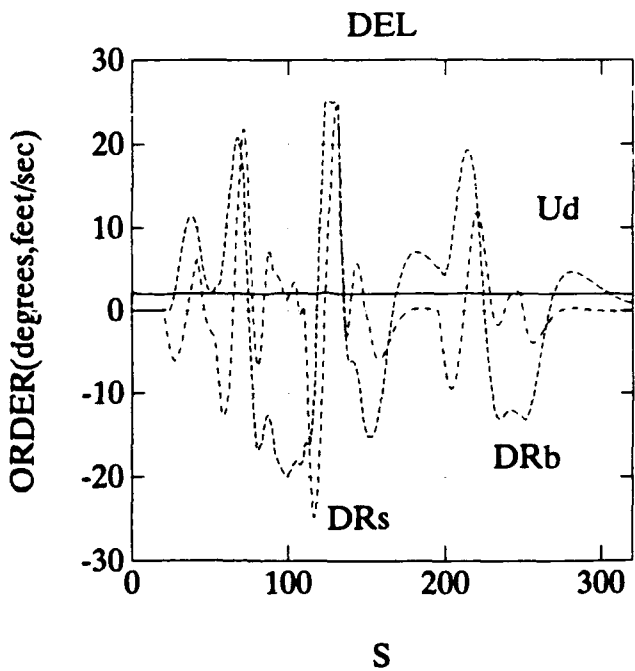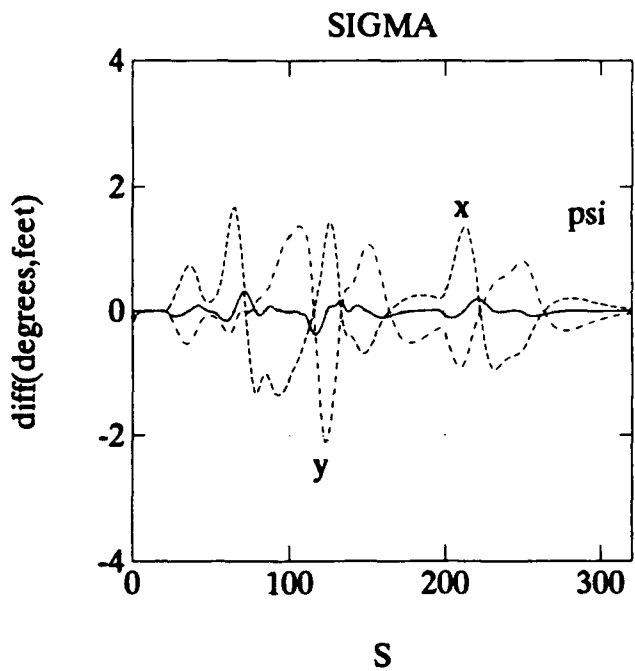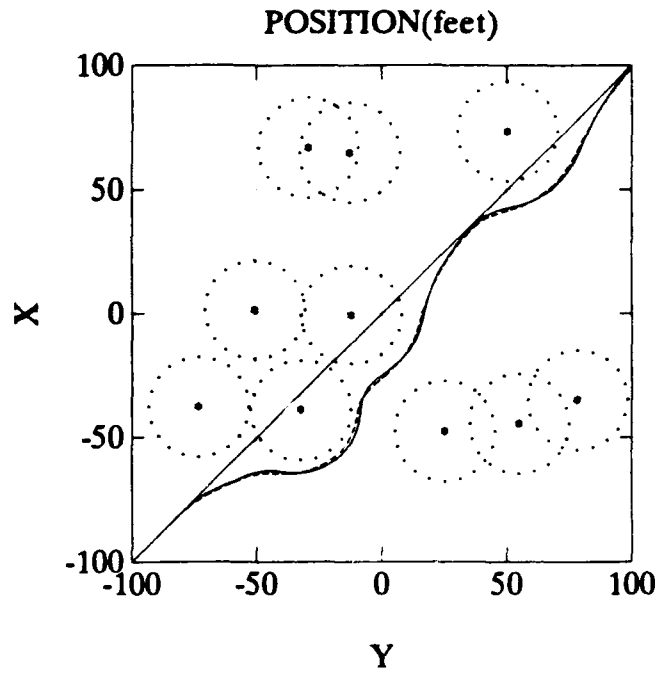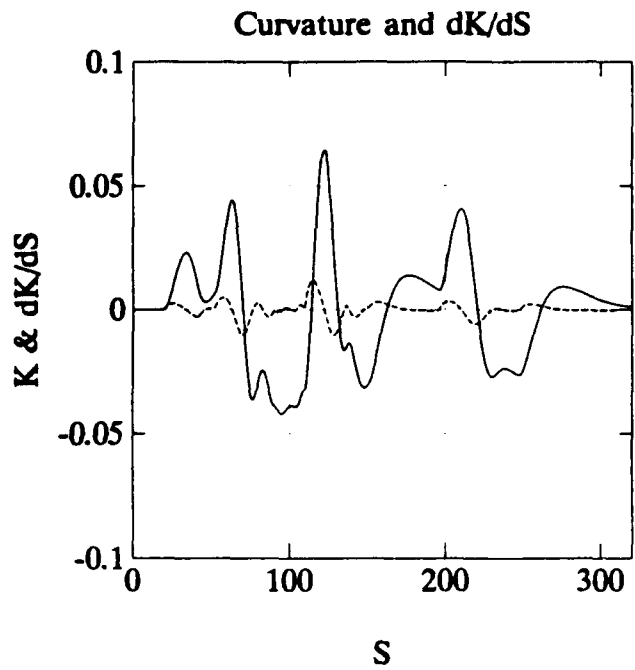
Figure V-5.   AUV Simulation: Obstacle Avoidance Ten Randomly Placed Mines

51

VL.   CONCLUSIONS AND RECOMMENDATIONS

A.   CONCLUSIONS

Nonlinear MIMO sliding mode control provides a useful framework for following a continuous curvature path. Though the errors produced following a curved path are larger compared to those experienced in linear path tracking, feasibility for use with AUVs has been demonstrated.

The use of curvature to create real time obstacle avoidance paths is possible. A simple reflexive mine avoidance algorithm has been developed which is easy to apply. But this simple reflexive algorithm has limitations. The magnitude and rate of curvature must be limited to the vehicle's dynamic capabilities and these values are speed dependent. When limiting curvature changes to the vehicle's dynamic capability, avoidance can not always be guaranteed. There is a maximum mine field density for the given vehicle's turning capabilities and a specified mine avoidance range.

Although only a few examples have been presented, in a large number of simulations during the course of this study, the combination of path generation and nonlinear control has been successfully demonstrated.

B. RECOMMENDATIONS

Since *DR* is proportional to K the use of curvature to directly command rudder orders should be evaluated. Combining curvature generated from the avoidance routine with a speed controller to reach the waypoints on time may be a simpler control system. This would bypass the need for the generation of a path. Though using only curvature commands may appear to be a simpler possibility for rudder control in a Mine Warfare situation, the primary thrust of this thesis was to develop an ability to follow curved paths. The Mine Warfare application was only used as an example.

The addition of thrusters on the AUV II this fall will significantly improve its maneuvering capability and allow operation in a higher density mine field. Implementation of thrusters into this control architecture should be attempted. Rule based control of the thrusters could be accomplished easily.

The selection of the sliding mode parameters is all trial and error. Future work should determine a sliding mode parameter prediction method that would take the "guesswork" out of parameter selection.

APPENDIX A.-COMPUTER CODE FOR NONLINEAR MIMO CONTROL

```
% PROGRAM EQNX3O2M.M
% THIS NON-LINEAR CONTROL PROGRAM FOR AUV USES 3X3 MIMO WITH
% CONTROLS (RPM^2,FWD RUDDER, AFT RUDDER)
% OBERVABLES (HEADING,GLOBAL X, GLOBAL Y) AND
% SLIDING MODE CONTROL (SIGMA=Y+LAMDA*Ydot)
% PATH GENERATED BY AVOID2.M AND STORED IN PATH.MAT
% USES RUDDER LIMITS OF 25 DEGREES
clear;
% CONSTANT PARAMETERS

Weight =435;
L       =87.625/12;
g       =32.2;
Mass    =Weight/g;
Izz     =45;
RHO     =1.94;
CDO     =0.015;
Umax    =2.3;                        % Turns per Knot ratio
RPMmax =500;                         % Max prop RPM
delt    =.1;                         % Time step
DRlim   =25/180*pi;

ETA=[20,0,0;
      0,10,0;
      0,0,10];
PSI=[1;10;10];
LAMDA=[.5,0,0;                       % Effectiveness of higher order terms
      0,5,0;
      0,0,5];

%load path
load c:\data\dean\matlab\cs4313\path     % Path to follow(YD, YDdot, YDdot2)
N=length(YD(1,:));
```

% HYDRODYNAMIC COEFFICIENTS

```
Xudot  =-0.00282*0.5*RHO*L^3;
Xuu    =CDO*0.5*RHO*L^2;
Xprop  =Xuu*(Umax/RPMmax)^2;
Yrdot  =-0.00178*0.5*RHO*L^4;
Yr     =+0.01187*0.5*RHO*L^3;
Yvdot  =-0.03430*0.5*RHO*L^3;
Yv     =-0.03896*0.5*RHO*L^2;
Ydrb   =+0.02345*0.5*RHO*L^2;
Ydrs   =+0.02345*0.5*RHO*L^2;
Nrdot  =-0.00047*0.5*RHO*L^5;
Nvdot  =-0.00178*0.5*RHO*L^4;
Nr     =-0.01022*0.5*RHO*L^4;
Nv     =-0.00769*0.5*RHO*L^3;
Ndrb   =+0.283*L*Ydrb;
Ndrs   =-0.377*L*Ydrs;


M=     [(Mass-Xudot),0,0,0,0,0;
        0,(Mass-Yvdot),0,0,0,0;
        0,0,(Izz-Nrdot),0,0,0;
        0,0,0,1,0,0;
        0,0,0,0,1,0;
        0,0,0,0,0,1];


H=     [0,0,0,1,0,0;
        0,0,0,0,1,0;
        0,0,0,0,0,1];
```

% INITIAL CONDITIONS

```
X(:,1)  =[2;0;0;YD(1,1);YD(2,1);YD(3,1)];
Xdot(:,1)=[0;0;0;YDdot(1,1);YDdot(2,1);YDdot(3,1)];


for i=1:N;


G=[Xprop,    0,                 0;
        0,    Ydrb*(X(1,i)^2),   Ydrs*(X(1,i)^2);
        0,    Ndrb*(X(1,i)^2),   Ndrs*(X(1,i)^2);
        0,    0,                 0;
        0,    0,                 0;
        0,    0,                 0];
```

```
F(:,i)=[(Mass*X(2,i)*X(3,i)-Xuu*X(1,i)*abs(X(1,i)));
        (-Mass*X(3,i)*X(1,i)+Yv*X(2,i)*X(1,i)+Yr*X(3,i)*X(1,i));
        (Nv*X(2,i)*X(1,i)+Nr*X(3,i)*X(1,i));
        X(3,i);
        X(1,i)*cos(X(4,i))-X(2,i)*sin(X(4,i));
        X(1,i)*sin(X(4,i))+X(2,i)*cos(X(4,i))];


Fs=sin(X(4,i));
Fc=cos(X(4,i));


Fx=[-2*Xuu*abs(X(1,i)),          Mass*X(3,i),  Mass*X(2,i),            0,    0,   0;
    -Mass*X(3,i)+Yv*X(2,i)+Yr*X(3,i), Yv*X(1,i),    (Yr-Mass)*X(1,i),       0,    0,   0;
        Nv*X(2,i)+Nr*X(3,i),     Nv*X(1,i),    Nr*X(1,i),              0,    0,   0;
        0,                       0,            1,                      0,    0,   0;
        Fc,                      -Fs,          0,      -X(1,i)*Fs-X(2,i)*Fc, 0,   0;
        Fs,                      Fc,           0,      X(1,i)*Fc-X(2,i)*Fs,  0,   0];


temp=H*X(:,i)-YD(:,i);
temp(1)=normal(temp(1));                    % Normalize THETA error +-pi
SIGMA(:,i)=temp+LAMDA*(H*inv(M)*(F(:,i))-YDdot(:,i));
DEL(:,i)=(inv(LAMDA*H*inv(M)*Fx*inv(M)*G)*...
        (-(H+LAMDA*H*inv(M)*Fx)*inv(M)*(F(:,i))+...
        YDdot(:,i)+LAMDA*YDdot2(:,i)...
        -ETA*tanh(SIGMA(:,i)./PSI)));


% REALITY LIMITS ON RPM & RUDDER
if abs(DEL(1,i))>RPMmax^2
        DEL(1,i)=RPMmax^2*DEL(1,i)/abs(DEL(1,i));
end;
if abs(DEL(2,i))>DRlim
        DEL(2,i)=DRlim*DEL(2,i)/abs(DEL(2,i));
end;
if abs(DEL(3,i))>DRlim
        DEL(3,i)=DRlim*DEL(3,i)/abs(DEL(3,i));
end;


Xdot(:,i+1)=inv(M)*(F(:,i)+G*DEL(:,i)+C);
X(:,i+1)=X(:,i)+Xdot(:,i+1)*delt;
X(4,i+1)=normal(X(' '));
end;
Xdot(:,i+1)=[];
X(:,i+1)=[];
finplot
```

```
% PROGRAM FINPLOT.M
% Plots the output from EQNX3O2M.M

clg,hold off;
w=[0:pi/10:2*pi];
circ=20*[sin(w)+j*cos(w)];
zdata=DATA(:,2)+j*DATA(:,1);
[circmesh,zdatmesh]=meshdom(circ,zdata);
circplot=circmesh+zdatmesh;

!del plot.met
% if memory in plotter if full use Z>=2 to reduce the # data points by that factor
Z=2
dels=.2                                    % Incremental distance of path(U*delt)
axis('square');
subplot(221);
axis([0,length(K)*dels,-.1,.1]);
plot([1:Z:length(K)]'*dels,K(1:Z:N));grid;
title('Curvature and dK/dS');
xlabel('S');ylabel('K & dK/dS');
hold on;
plot([1:length(K)-1]'*dels,(K(2:N)-K(1:N-1))/dels,'--');
hold off;

subplot(222);
%axis([-10,140,-10,140]);
axis([-50,50,-50,50]);
%axis([-100,100,-100,100]);
plot(X(6,1:Z:N),X(5,1:Z:N),YD(3,1:Z:N),YD(2,1:Z:N));grid;
title('POSITION(feet)');
xlabel('Y');ylabel('X');
hold on;
plot([-100,100],[-100,100]);
plot(DATA(:,2),DATA(:,1),'*');
for i=1:length(circplot(1,:))
      plot(circplot(:,i),'.');
end;
hold off;
```

57

```
subplot(223)
axis([0,length(DEL(1,:))*dels,-4,4]);
plot([1:N]'*dels,SIGMA(1,:)*180/pi,'-r');
hold on
plot([1:Z:N]'*dels,SIGMA(2,1:Z:N),'--g');
plot([1:Z:N]'*dels,SIGMA(3,1:Z:N),'-.b');
grid;title('SIGMA');
gtext('psi');
gtext('x');gtext('y');
xlabel('S');ylabel('diff(degrees,feet)');
hold off

subplot(224)
axis([0,length(DEL(1,:))*dels,-30,30]);
plot([1:N]'*dels,Umax/RPMmax*sqrt(DEL(1,:)),'-r')
hold on
plot([1:Z:N]'*dels,DEL(2,1:Z:N)*180/pi,'--g');
plot([1:Z:N]'*dels,DEL(3,1:Z:N)*180/pi,'-.b');
title('DEL');xlabel('S');ylabel('ORDER(degrees,feet/sec)');grid;
gtext('Ud');
gtext('DRb');
gtext('DRs');
hold off
meta plot;
```

58

APPENDIX B.-COMPUTER CODE FOR PATH GENERATION

```
% PROGRAM AVOID2.M
% Generates a path following a nominal path while avoiding a mine field.
clear;

hold off;
clg;
load DATA                           % Loads current mine field data file

axis([-100,100,-100,100]);
plot(DATA(:,1),DATA(:,2),'+r');
title('MINE AVOIDANCE/LOCALIZATION');
xlabel('X');ylabel('Y');            % Plot mine field
hold on;
X1=-50;
Y1=-50;                             % Path start position
X2=50;
Y2=50;                              % Path finish position

m=(Y2-Y1)/(X2-X1);                  % Slope of path
THETAim=atan2(Y2-Y1,X2-X1);         % Orientation of path
b=Y1-m*X1;                          % Y intercept of line
Kim=0;                              % Curvature of path

delt=.1;                            % path increments
U=2;
dels=U*delt;
N=800;                              % number of data  points
L=N*dels;                           % Initial length of arc
k=.1;                               % Manuever sharpness factor

THETA(1)=pi/4;                      % Initial conditions
X(1)=-50;
Y(1)=-50.00001;
s(1)=0;
K(1)=1e-10;
delK(1)=0;
```

59

```
for i=1:N,                                  % Calculations for intercept
    s(i+1)=s(i)+dels;                       % Path position
                                            %Distance to path calculation
    D(i)=sqrt((m^2*X(i)-m*(Y(i)-b))^2+(Y(i)-X(i)*m-b)^2)/(m^2+1);

    if atan2(Y(i)-Y1,X(i)-X1)<THETAim,      % Determines L/R of line
        D(i)=-D(i);
    end;


    delKp(i)=-(3*k*(K(i)-Kim)+3*k^2*normal(THETA(i)-THETAim)+k^3*D(i));

% call Sensor routine to determine if mine is detected and orders delK to avoid


    sensor_m


        delK(i)=delKp(i)+delKa(i);          %Total delK
                                            % Limit on delK to ensure continuous K
        if abs(delK(i))>0.005, delK(i)=.005*abs(delK(i))/delK(i); end;
        K(i+1)=K(i)+delK(i)*dels;
        if abs(K(i+1))>0.050, K(i+1)=.050*abs(K(i+1))/K(i+1); end;
        THETAdot(i)=K(i)*U;                 % THETA Rate
        delTHETA(i)=THETAdot(i)*delt;       % Change in THETA
        d=dels*(sin(delTHETA(i)/2)/(delTHETA(i)/2));   % Distance linear in delt
        THETA(i+1)=THETA(i)+delTHETA(i);    % New THETA
        Xdot(i)=U*cos(THETA(i)+delTHETA(i)/2);   % X Rate
        X(i+1)=X(i)+Xdot(i)*delt;           % New X
        Ydot(i)=U*sin(THETA(i)+delTHETA(i)/2);   % Y Rate
        Y(i+1)=Y(i)+Ydot(i)*delt;           % New Y
    plot(X(i),Y(i),'*')
end
                                            % Euler estimates of accelerations
        Xdot2=([0,Xdot]-[Xdot,0])/delt;
        Ydot2=([0,Ydot]-[Ydot,0])/delt;
        THETAdot2=([0,THETAdot]-[THETAdot,0])/delt;
YD=[THETA;X;Y];                             % Generate path data
YDdot=[THETAdot;Xdot;Ydot];
YDdot2=[THETAdot2;Xdot2;Ydot2];
YD(:,N+1)=[];
YDdot2(:,N+1)=[];
s(N+1)=[];
K(N+1)=[];
save path YD YDdot YDdot2 K                 % Save data for future evaluation
avoidplt                                    % Call plot routine
```

60

```matlab
% PROGRAM SENSOR_M.M
% Input: DATA(i),i,X,Y
% Output: delKa(i),
% Subroutine to determine delK to avoid mines detecable by sensors

Kscale=.05;                                 % Scaling factor
Rhsensor=50;                                % Range of detection
Rhavoid(i)=20;                              % Min allowed range to mine
BRGdet=[];                                  % Initialize routine
Rhdet=[];
count=0;
                                            % Distance to all mines
Rh(i,:)=sqrt((((DATA(:,1)-X(i)).^2)+((DATA(:,2)-Y(i)).^2))';

[Rhmin(i),I(i)]=min(Rh(i,:));               % Distance to nearest mine
if i>1;
for c=1:length(DATA(:,1));                  % Find all mines within Rhdet
   if Rh(i,c)<=Rhsensor & Rh(i,c)<Rh(i-1,c)
     DATA(c,3)=DATA(c,3)+1;                 % # detects on each mine
     count=count+1;
     Rhdet(count)=Rh(i,c);
     BRGdet(count)=normal(atan2((DATA(c,2)-Y(i)),(DATA(c,1)-X(i)))-THETA(i));
   end;
end;
end;
if count>0                                  % Mine Detected
   delKr=abs((Rhsensor-Rhdet)./(Rhdet-Rhavoid(i)));      % Range Correction
   delKb=1-abs(BRGdet)*2/pi;                % Linear Bearing Corr
   delKa(i)=-sum(delKr.*delKb.* abs(BRGdet)./BRGdet)*Kscale; % delK for Avoidance
else
   delKa(i)=0;                              % No mine detected
end;
```

61

```
%PROGRAM AVOIDPLT.M plotting routine for PROGRAM AVOID.M
% Inputs: Rhavoid,DATA(X,Y),LOWLEFT,UPRIGHT,RHmin,s,K,delK
w=[0:pi/10:2*pi];                          % Generate avoidance circles
circ=20*[sin(w)+j*cos(w)];
zdata=DATA(:,2)+j*DATA(:,1);
[circmesh,zdatmesh]=meshdom(circ,zdata);
circplot=circmesh+zdatmesh;

!del plot.met;
hold off;
clg;
axis('square');
axis([-50,50,-50,50]);
subplot(211)                               % Position plot
plot(Y,X,[Y1,Y2],[X1,X2],DATA(:,2),DATA(:,1),'*r');
title('PATH');xlabel('Y');ylabel('X');
grid;
hold on;
plot(circplot,'.');
hold off;

subplot(223);          % Range plot
axis([0,max(s),0,100]);
plot(s,Rhmin,s,Rhavoid);title('Rhmin & Rhavoid');
xlabel('S');ylabel('Rh');
grid;

subplot(224);                              % Curvature plot
axis([0,max(s),-.1,.1]);
plot(s,K,s,delK);title('Curvature & dK/dS');
xlabel('S');ylabel('K & dK/dS');
grid;
meta plot;
```

LIST OF REFERENCES

1. Healey, A. J., and Lienard., D., "Multivariable Sliding Mode Control for Autonomous Diving and Steering of Unmanned Underwater Vehicles", *IEEE Journal of Oceanic Engineering*, Vol. 18, No. 3, pp.1-13, July 1993.

2. Slotine, J. J. E., and Li, W., *Applied Nonlinear Control*, Prentice Hall, 1991.

3. Healey, A. J., and Good, M., "The NPS AUV II Autonomous Underwater Vehicle Testbed: Design and Experimental Verification", *Naval Engineers Journal*, ASNE, pp.191-202, May1992, .

4. Byrnes, R., Kwak, S. H., McGhee, R. B., and Healey, A. J., "Rational Behavior Model: An Implemented Tri-level Multilingual Software Architecture for Control of Autonomous Underwater Vehicles", Proceedings of the 8th International Symposium on Unmanned Untethered Submersible Technology, 27-29 September 1993.

5. Lewis, E. V. (Ed), *Principles of Naval Architecture*, Society of Naval Architects and Marine Engineers, April 1988.

6. Warner, D. C., *Design,Simulation, and Experimental Verification of a Computer Model and Enhanced Position Estimator for the NPS AUV II*, Master's Thesis, Naval Postgraduate School, Monterey, California, December 1991.

7. Kanayama, Y., *Introduction to Spacial Reasoning*, Naval Postgraduate School, Monterey, California, September 1992.

8. Bahrke, F. G., *On Line Identification of the Speed, Steering, and Diving Response Parameters of an Autonomous Underwater Vehicle from Experimental Data*, Master's Thesis, Naval Postgraduate School, Monterey, California, March 1992.

9. Hawkinson, T, D., *Multiple Input Sliding Mode Control for Autonomous Diving and Steering of Underwater Vehicles*, Master's Thesis, Naval Postgraduate School, Monterey, California, December 1990.

10. Healey, A. J., *Dynamics of Marine Vehicles*, Naval Postgraduate School, Monterey, California, October 1992.

11. Sur, J.-N., *Design and Investigation of a Dive Plane Sliding Mode Compensator for an Autonomous Underwater Vehicle*, Master's Thesis, Naval Postgraduate School, Monterey, California, September 1989.

INITIAL DISTRIBUTION LIST

1. Defense Technical Information Center   2
   Cameron Station
   Alexandria, VA 22304-6145

2. Library, Code 52   2
   Naval Postgraduate School
   Monterey, CA 93943-5002

3. Chairman, Code ME   1
   Department of Mechanical Engineering
   Naval Postgraduate School
   Monterey, CA 93943-5000

4. Dr. Anthony J. Healy, Code ME/HY   2
   Department of Mechanical Engineering
   Naval Postgraduate School
   Monterey, CA 93943-5000

5. Professor Yutaka Kanayama, Code CS/Ka   1
   Department of Computer Science
   Naval Postgraduate School
   Monterey, CA 93943-5000

7. Technical Library   1
   Naval Surface Warfare Center
   Silver Springs, Maryland 20901

8. LCDR Donald P.Brutzman, Code OR/Br   1
   Naval Postgraduate School
   Monterey, CA 93943-5000

9. LCDR Bill Flynn   1
   CNO Code N85
   ATTN: N852 Rm 5E613
   Pentagon, Wasington, D.C. 20350-5000

10. CAPT Alan R. Beam   1
    ARPA
    3701 N. Fairfax DR.
    Arlington, VA 22203-1714

11. Claude P. Brancart   1
    C. S. Draper Labs, Inc.
    4301 N. Fairfax DR. Ste 700
    Arlington, VA 22203

12. CAPT Kenneth L. Cottle   1
    30718 SE 358th ST.
    Enumclaw, WA 98022

13. LCDR Dean J. Cottle, USN   1
    Supervisor of Shipbuilding
    Naval Submarine Base
    Groton, CT 06340